On the Role of the Bridging Dicyanamidobenzene Ligand in a New Binuclear Ruthenium Complex: [Ru(tpy)(thd) 2 (μ-dicyd)][PF 6] with tpy = 2,2‘:6‘,2‘ ‘-Terpyridine and thd = 2,2,6,6-Tetramethyl-3,5-heptanedione

Muriel Fabre, Joël Jaud, Mohamed Hliwa, Jean-Pierre Launay, Jacques Bonvoisin

On the Role of the Bridging Dicyanamidobenzene Ligand in a new Binuclear Ruthenium Complex: $[\{Ru(tpy)(thd)\}_2(\mu\text{-dicyd})][PF_6]$ with tpy = 2,2':6',2"-terpyridine, thd = 2,2,6,6-tetramethyl-3,5-heptanedione.

Muriel Fabre,[a] Joël Jaud,[a] Mohamed Hliwa,[a,b] Jean-Pierre Launay, [a] and Jacques Bonvoisin[*,a]*

Contribution from the [a] CEMES/CNRS, NanoSciences Group, BP 94347, 29 rue Jeanne Marvig, 31055 Toulouse cedex 4, France ; and [b] Faculté des Sciences, Université Hassan II-Mohammédia, BP 7955-Sidi Othman, Casablanca, Maroc.

Keywords : Non innocent bridging ligand, Mixed-valence, Electron-transfer, Ruthenium complexes, dicyanamidobenzene, Hole-transfer, X-ray structure, Electrochemical properties, Spectroelectrochemistry, EPR spectroscopy, DFT calculation.

Corresponding author: CEMES/CNRS, NanoSciences Group, BP 94347, 29 rue Jeanne Marvig, 31055 Toulouse cedex 4, France Tel. : +33 5 62 25 78 52, fax: +33 5 62 25 79 99, jbonvoisin@cemes.fr

Abstract

The dicyanamidobenzene-bridge diruthenium complex [{Ru(tpy)(thd)}$_2$(μ-dicyd)][PF_6] ([**3**][PF_6]) {dicyd = 1,4-dicyanamidobenzene, tpy = 2,2':6',2"-terpyridine, thd = 2,2,6,6-tetramethyl-3,5-heptanedione} and its mononuclear counterpart [Ru(tpy)(thd)(Ipcyd)] (**2**) {Ipcyd = 4-iodophenylcyanamide anion ($Ipcyd^-$)} were synthesized and fully characterized. Cyclic voltammetry of **3** showed the presence of four reversible one-electron redox couples. UV-Visible-NIR spectroelectrochemistry and EPR spectroscopy of the electrogenerated paramagnetic intermediates were used to ascertain the oxidation-state distribution. The stable starting dinuclear complex $\mathbf{3}^+$ is found to be a ligand-centered anion radical as shown by EPR spectroscopy, magnetic susceptibility measurements, and DFT calculations. Oxidation of $\mathbf{3}^+$ to $\mathbf{3}^{2+}$ led to a EPR silent system due to substantial intramolecular antiferromagnetic interaction of the electron spins carried by the low spin ruthenium(III) atom and the bridging anion radical dicyanamido ($dicyd^{\bullet-}$), an observation which was supported by UV/Vis/NIR, X-Ray structure and DFT calculations. $\mathbf{3}^{3+}$ presented a EPR spectra consistent with a total effective spin S=1/2 issued from an antiferromagnetic interaction of electron spins carried by two low spin ruthenium(III) atoms and the bridging anion radical $dicyd^{\bullet-}$ in accordance with UV/Vis/NIR. This study shows that the dicyanamidobenzene bridging ligand has indubitably a non-innocent behavior.

1 Introduction

The development of newer classes of dinuclear metal complexes incorporating suitable bridging ligands which lead to the formation of stable mixed valence (MV) states has attracted considerable research in recent years.[1, 2] This was primarily due to the relevance for biological processes,[3] molecular electronics,[4] and theoretical studies of electron transfer kinetics.[5] The bridging ligand (BL) mediated intermetallic electronic communication takes place through their π-symmetry orbitals either by electron-transfer (ET) or hole-transfer (HT) mechanisms.[6]

Dicyanamidobenzene ligands are proned to be well suited for intramolecular electro- and magnetocommunications [7-10] via a HT mechanism. [7, 10-13] To achieve a strong electronic interaction it is necessary to match the energy of the metal-based redox orbital with an appropriate BL orbital, such that delocalization in the MV state can be optimized by a superexchange process involving the BL: here, HT through the BL HOMO (Highest Occupied Molecular Orbital). A fundamental question is to know if such a ligand is innocent or not during this process. [14] Such a question has already been addressed by several groups [1, 14-17] and very recently on bridging arylethynyl ligand [18] in binuclear ruthenium and iron complexes. In this study, we will focus on the non-innocent behavior of the dicyanamidobenzene BL. We report here the synthesis of $[\{Ru(tpy)(thd)\}_2(\mu\text{-dicyd})]^+$, [**3**]($PF_6$) with tpy = 2,2':6',2"-terpyridine, thd = 2,2,6,6-tetramethyl-3,5-heptanedione, including the crystal structure in its +2 form, and the electrochemical and spectroscopic properties with detailed spectroelectrochemical studies over a wide range of accessible oxidation states as well as EPR and magnetic susceptibility measurements and computational investigations. The combination of all these studies gives some information on the frequently debated question for such systems, *i.e*. which is the oxidation site?

2 Results

2.1 Synthesis

The syntheses of **1** and **2** were adapted from literature procedures.[19] The mononuclear complex **2** could then be obtained from **1**. The chloride ligand is easily displaced by adding silver hexafluorophosphate in a refluxing mixture of ethanol and water and the resulting silver chloride precipitate can be eliminated by filtration. Addition of 10 equivalents of 4-iodophenylcyanamide ligand leaded to complex **2** in a rather good yield. (See scheme 1)

Insert Scheme 1

The dinuclear complex [**3**][PF_6] could be obtained via the same route (removal of the chloride ligand followed by complexation of the dicyanamide bridging ligand). (See scheme 1) The first oxidizing potential of the complex being very low (-0.24V vs. SCE in CH_2Cl_2, 0.1M TBAHFP), after purification the complex is obtained in its monooxidized form as a hexafluorophosphate salt.

Chemical oxidation of the mononuclear complex **2** was performed in dichloromethane using ferrocenium hexafluorophosphate as an oxidizing agent. The corresponding hexafluorophophate salt of the Ru(III) form of complex **2** was obtained. The possible excess of oxidizing agent could be easily removed by filtration through celite and the ferrocene sideproduct was eliminated by precipitation of the oxidized complex in a dichloromethane/cyclohexane mixture, filtration and washing with cyclohexane.

Chemical oxidation of the dinuclear complex [**3**][PF_6] was also performed under the same conditions to obtain the dicationic form of the dinuclear complex.

2.2 Electrochemistry

Cyclic voltammograms (CV) and Differential pulse voltammograms (DPV) of the complexes were recorded in dichloromethane, dimethylformamide and/or acetonitrile under an argon atmosphere with 0.1 M tetrabutylammonium hexafluorophosphate (TBAH). The $E_{1/2}$ potentials were determined from the average of the anodic and cathodic peak potentials for reversible waves. For irreversible waves, only the anodic peak potentials are reported.

The CV of complex **1** showed only one reversible wave in oxidation (at 0.198 V in dichloromethane and 0.249 V in dimethylformamide). This wave was assigned to the Ru(III/II) couple [20] and is slightly shifted toward the cathodic potentials compared to the equivalent complex [Ru(tpy)(acac)Cl] (0.288 V in dimethylformamide) due to the addition of donor methyl groups on the acetylacetonate ligand.

The CV of complex **2** showed two waves in oxidation. The first quasi-reversible wave at 0.200 V corresponds to the Ru(III/II) couple. The second irreversible wave at 1.064 V was attributed to the oxidation of the cyanamide ligand. [20, 21] This last point is consistent with the absence of this wave on the voltammogram of compound **1**, which does not contain this ligand.

The CV of dinuclear complex [**3**][PF_6] presents three reversible waves in oxidation and one reversible wave in reduction (*cf.* Figures 1, S1 and Table 1). Four redox couples can be considered : each metal can be reversibly oxidized once from Ru(II) to Ru(III) and the dicyanamidobenzene bridging ligand can also be reversibly oxidized twice [7, 9] as shown below :

$$Ru^{II}\text{-}Ru^{II} \underset{E_{M1}}{\overset{-e^-}{\rightleftharpoons}} Ru^{II}\text{-}Ru^{III} \underset{E_{M2}}{\overset{-e^-}{\rightleftharpoons}} Ru^{III}\text{-}Ru^{III} \; ; \; L^{2-} \underset{E_{L1}}{\overset{-e^-}{\rightleftharpoons}} L^{\bullet -} \underset{E_{L2}}{\overset{-e^-}{\rightleftharpoons}} L^{0}$$

This behavior is very similar to that of other complexes presenting the dicyanamidobenzene dianion as a bridging ligand (see Table 1). Note that the potentials are anodically shifted when an amino group NH_3 in $[\{Ru(NH_3)_5\}_2(\mu\text{-dicyd})][PF_6]_4$ is replaced by π-acceptor ligands such as polypyridyle ligands. For complex **3** containing a terpyridine ligand along with an electron donor ligand thd, its potential should be expected to be intermediate between those of $[\{Ru(NH_3)_5\}_2(\mu\text{-dicyd})][PF_6]_4$[12] and $[\{Ru(tpy)(bpy)\}_2(\mu\text{-dicyd})][PF_6]_2$ [9] as it is actually the case.

Insert Figure 1

Insert Table 1

2.3 Electronic absorption

Electronic absorption data are summarized in Table 2. For $dicyd^{2-}$, spectroelectrochemical oxidation analysis was already done [9] but was reproduced here in DCM for the sake of comparison (See also Figure S2)

Insert Table 2

The spectra of complexes **1** and **2** in DCM showed two broad bands in the visible region (around 570 nm), which can be assigned to dπ(Ru(II)) → π*(tpy) MLCT transitions.[20] The two intense bands (around 280 and 320 nm) are attributable to π → π* transitions of the terpyridine ligand.

Upon oxidation of complex **2**, the two broad bands around 570 nm disappeared and a more intense band appeared at 1005 nm. This transition is absent in complex $\mathbf{1}^+$, which indicates that it implies the $Ipcyd^-$ ligand. We assigned it to a π(Ipcyd)→ dπ(Ru(III)) LMCT transition. This was previously observed in oxidized complexes of the [Ru(tpy)(acac)] family. [20]

The dinuclear complex [**3**][PF_6] also showed two broad bands around 530 nm which can be assigned to dπ(Ru(II) → π*(tpy) MLCT transitions and two intense bands (around 280 and 320 nm) which are attributable to π → π* transitions of the terpyridine ligand. These bands are almost twice as intense as

the corresponding bands in the two mononuclear compounds, which is in agreement with the attribution proposed here. Complex [**3**][PF_6] also presented an additional transition at 380 nm, which we tentatively assigned to the dicyanamidobenzene bridging ligand, and a broad, intense and low energy transition at 1366 nm, the attribution of which will be discussed later.

2.4 UV/Vis/Near-IR Spectroelectrochemistry

Spectroelectrochemical studies of dinuclear complex [**3**][PF_6] were performed in DCM (see Table 2) and also in acetonitrile and DMF to generate the spectra of the neutral form **3** and the charged forms $\mathbf{3}^{2+}$, $\mathbf{3}^{3+}$ and $\mathbf{3}^{4+}$ of the dinuclear complex and are shown in Figure 2. (See also Figures S3-S6)

Insert Figure 2

Upon reduction of dinuclear complex [**3**][PF_6] to its neutral form, the broad and intense transition at 1366 nm disappears as well as the narrower transition at 380 nm.

During the electrochemical oxidation of dinuclear complex **3** from the charged form $\mathbf{3}^{+}$ to the charged form $\mathbf{3}^{2+}$, the transition at 1366 nm is shifted toward higher energies (1290 nm) and the transition at 380 nm disappears.

During the electrochemical oxidation from the charged form $\mathbf{3}^{2+}$ to the charged form $\mathbf{3}^{3+}$, the transition at 1290 nm disappears and a thinner but as intense transition appears at 1018 nm.

During the electrochemical oxidation from the charged form $\mathbf{3}^{3+}$ to the charged form $\mathbf{3}^{4+}$, the transition at 1018 nm disappears.

2.5 EPR spectra

The EPR spectrum of [**2**][PF_6] (See Figure S7) is a very typical rhombic spectrum of a low spin d^5 Ru(III) ion [22] with three well resolved components: $g_1 = 2.48$, $g_2 = 2.13$ and $g_3 = 1.81$. This gives the average g value of 2.16 ($\langle g \rangle = [(g_1^2+g_2^2+g_3^2)/3]^{1/2}$) which is in very good agreement with the g value obtained by magnetic susceptibility measurements (see below). This average g value is a bit smaller than the one obtained for $[Ru(tpy)(acac)Ipcyd]^+$ which is found to be 2.19 with $g_1 = 2.55$, $g_2 = 2.17$, $g_3 = 1.79$. [23] The smaller <g> value for $\mathbf{3}^{+}$ can be attributed to the stronger donor character of thd compared

to acac as it has already been observed on a series of dinuclear ruthenium complexes with various donor substituents. [16]

Insert Figure 3

The EPR spectrum of [**3**] [PF_6] (Figure 3) showed the signal of an isotropic system with g = 2.02 with a peak to peak separation of 60 G. This is characteristic of a radical species which indicates unique participation of the bridging ligand in the spin distribution.[16, 24] This clearly rules out the [Ru^{II}(μ–dicyd^{2-})Ru^{III}] formulation and favour the radical one [Ru^{II}(μ–dicyd$^{\bullet-}$)Ru^{II}] instead. One can also compare this spectrum to the one observed for potassium salt of dicyd$^{\bullet-}$**,** which is centered at g = 2.0034 and presents hyperfine coupling of around 1-5 Gauss. [25] The spectrum observed for [**3**] [PF_6] does not present any hyperfine coupling but is very similar to the one observed for the silver salt of DI-dicyd$^{\bullet-}$ (where DI-dicyd$^{\bullet-}$ = 2,5-diiodo-1,4-dicyanamidobenzene anion), where the absence of hyperfine coupling can be explained by interactions between the anion radical π system and the metallic d orbitals. [26]

Insert Figure 4

The EPR spectrum of **3**$^{3+}$ showed the signal of an isotropic system with g = 2.08 with a peak to peak separation of 290 G, which is five times broader than the signal of **3**$^{+}$.

2.6 Magnetic measurements

We carried out variable-temperature (2-50 K) magnetic studies of powder samples of complexes **2**$^{+}$ and **3**$^{+}$. The product of magnetic susceptibility (χ) with the temperature (T) versus T for both compounds are shown on Figure 5. Both compounds follow the Curie law down to 10 K. Below this temperature, the product (χT) slightly decreases due to inter-molecular antiferromagnetic interactions. Using the Curie-Weiss equation [27] (equation 1), we found g = 2.20 and θ = -0.40K for **2**$^{+}$ and g = 1.95 and θ = -0.40K for **3**$^{+}$. Interestingly, the Curie constant for complex **2**$^{+}$ was found to be C = 0.44 $cm^3.mol^{-1}K$ (μ_{eff} = 1.88μ_B), which is very typical of a low spin ruthenium(III) S=1/2 state,[28] and for

complex $\mathbf{3}^{+}$ we found C = 0.35 $cm^3.mol^{-1}K$ (μ_{eff} = 1.67μ_B), which is much closer to a typical radical S=1/2 state with g = 2.0, C = 0.375 $cm^3.mol^{-1}K$ and μ_{eff} = 1.732μ_B.

$$\chi_M = \frac{Ng^2\mu_B^2 S(S+1)}{3k(T-\theta)} \quad (1)$$

Insert Figure 5

2.7 X-ray Crystallography

The ORTEP diagram of complex [**3**][PF_6]$_2$ is shown in Figures 6 and 7. The hexafluorophosphate counter anions were omitted for the sake of clarity. Crystallographic data are shown on Table 3 and selected bond lengths and angles are given in supplementary materials. The particularity of this structure is the presence of two independent molecules, conformers A (Figure 6) and B (Figure 7). The cyanamide groups are in an anti configuration as it has already been seen in similar systems. [7, 10] Each of these two molecules is centrosymmetric with a centre of symmetry on the central phenyl ring of the bridging ligand. Their structures are very similar. This led us to check the accuracy of the space group by the use of PLATON, which confirmed that the chosen group was the good one. There are two types of $\mathbf{3}^{2+}$ in the unit cell (conformers A and B), which crystallized on two symmetry positions ; as Z = 8, this makes 4 + 4 = 8 complexes $\mathbf{3}^{2+}$ per unit cell. There are three types of PF_6^-, one type lies on a general position and the two other types lie on two symmetry positions, which makes 8 + 4 + 4 = 16 PF_6^- per unit cell (See Figure S8).

Insert Figures 6 and 7

Insert Table 3

3 Discussion

The cyclic voltammogram of dinuclear complex [**3**][PF_6] presents three reversible waves in oxidation and one reversible wave in reduction. Four redox couples can be considered: each metal can be reversibly oxidized once from Ru(II) to Ru(III) and the dicyanamidobenzene bridging ligand ($dicyd^{2-}$) can also be reversibly oxidized twice to form a radical anion species ($dicyd^{\cdot-}$) and a neutral species ($dicyd^0$).

To sum up, the dinuclear complex **3** presents four reversible waves in electrochemistry and four redox couples can be considered. The title complex was obtained in its monooxidized form, but for pedagogical purposes, it is clearer to start from the fully reduced $\mathbf{3}^0$ species and look at its behavior upon progressive oxidation. The question is which part of the complex is oxidized first? How can we assign each redox couple to each wave? If one looks at every possible electronic structure for each oxidation step, one notices that this is a complicated system with a very rich behavior in oxidation (Scheme 2).

Insert Scheme 2

Note that the highest complexity occurs for the intermediate oxidation state $\mathbf{3}^{2+}$, for which three different electronic structures can be written.

In order to answer the difficult problem of the site of oxidation, we have analyzed the experimental results along with the theoretical ones. Calculations were performed for the first three members of the series, i.e. **3**, $\mathbf{3}^+$ and $\mathbf{3}^{2+}$. There are several ways to answer to this question using the output of DFT calculations : (i) using the variation of atomic charges, computed according to either Mulliken or Lowdin rules, (ii) using the spin densities, in the case of an open-shell system such as $\mathbf{3}^+$, and (iii) using molecular orbital diagrams and the correlation from one compound to the other. Method (iii) is in principle less satisfactory since the DFT method does not rely on the concept of molecular orbitals, and is actually designed to deal with the total charge density.

3.1 The neutral complex 3

In its neutral form, the dinuclear complex presents formally two ruthenium(II) centers linked to two neutral tpy ligands, two anionic thd ligands and a dianionic bridging ligand $dicyd^{2-}$. Upon reduction of dinuclear complex [**3**][PF_6] to its neutral form $\mathbf{3}^0$, the characteristic UV-Vis spectrum of a Ru(II) complex is recovered, with two broad bands in the visible region, which can be assigned to $d\pi(Ru(II)) \rightarrow \pi^*(tpy)$ MLCT transitions. The ground state of the complex is thus a closed shell singlet. The HOMO of the complex (Figure 8) is predominantly localized on the bridging ligand dicyd, with a contribution of 89 %. This first result is in favour of the oxidation of the bridging ligand before the

oxidation of the metal, as shown experimentally by the EPR spectrum of complex $\mathbf{3}^{+}$. Of course one has to be careful with conclusions drawn from the sole inspection of the HOMO, because orbital reorganization can occur once the complex is oxidized. But this conclusion is supported by calculations on the mono-oxidized form (see below).

Insert Figure 8

Interestingly, the structure of the bridging ligand in complex **3** is very similar to the optimized geometry of the free $dicyd^{2-}$ ligand, the largest deviation for the computed bond lengths a, b, c and d being only 0.01 Å. This indicates that the benzenic ring of the ligand is almost unchanged upon complexation.

3.2 The monooxidized form 3^{+}

If the metal was oxidized first, $\mathbf{3}^{+}$ could be the mixed-valence form of the complex (Ru^{II}-$dicyd^{2-}$-Ru^{III}). The broad, intense and low energy transition at 1366 nm on the electronic absorption spectrum could then be attributed to an intervalence transition. On the other hand, if the ligand is oxidized first (Ru^{II}-$dicyd^{\bullet-}$-Ru^{II}), this transition could be a $d\pi(Ru(II)) \rightarrow \pi^*(dicyd^{\bullet-})$ metal to ligand charge transfer transition (MLCT). One could object that if the ligand is oxidized first, one should observe the radical anion chromophore which presents four bands in the range of 300-700 nm, [9] but these bands are probably masked by the above described MLCT transitions which are four or five times more intense (See figure S2). Here, the electronic absorption spectrum is not enough to conclude.

However, the EPR spectrum of [**3**] [PF_6] showed the signal of an isotropic system with g = 2.02. This is very characteristic of a radical species, which seems to indicate that the radical anion form of the bridging ligand is prefered, which means that the ligand is oxidized first. Moreover, supposing the metal would be oxidized first to form a mixed-valence species, it has to be remembered that even a class III mixed-valence complex would keep the characteristics of a Ru(III), that is to say a rhombic signal.[29] This should be true whatever the transfer mechanism is (ET or HT). There is then evidence that the ligand is oxidized first. Magnetic susceptibility measurement is completely in agreement with this point

showing an effective magnetic moment much closer to a radical S = 1/2 spin state with g close to 2.0, rather than a ruthenium(III) low spin S = 1/2 which would have a larger g value close to g = 2.2. Other examples of radical anions as ligands [30] can be found in the literature but they are rather scarce as bridging ligands. [16, 17, 24]

For the theoretical study of $\mathbf{3}^{+}$, a full geometry optimization was performed at the Unrestricted Hartree-Fock level (UHF). The spin contamination was found to be negligible with $\langle S^2 \rangle = 0.764$, which differs from the theoretical value $\langle S^2 \rangle = S(S+1) = 0.750$ by less than 2 %.

Comparing the structure of the bridging ligand in complex $\mathbf{3}^{+}$ to the computed structure of the radical anion $L^{\cdot -}$ shows only very slight differences, the largest deviation for the computed bond lengths a, b, c and d being only 0.004 Å. The evolution of the atomic charges shows the same trend, with a charge 1+ distributed mainly on the bridging ligand (59 %), the two tpy ligands (28 %) and the two thd ligands (14 %).

The presence of an anion radical bridging ligand is also supported by the computed total spin density on the bridging ligand, which amounts to 0.90, clearly indicating that the bridging ligand was oxidized while the two ruthenium centers remained essentially untouched.

Insert Figure 9

Looking now at the molecular orbitals, since the calculations are performed in a self-consistent way on the oxidized form, the shape of the SOMO carries also some information on the site where oxidation has occurred. As shown in Figure 9, the SOMO resembles the HOMO of **3**, in agreement with a ligand-based oxidation. However, it has to be noticed that the proportion of the bridging ligand in this orbital, though still very significant (74 %), has slightly decreased upon oxidation (*cf.* 89 % in the HOMO of **3**).

3.3 The dioxidized form 3^{2+}

The electrochemical oxidation of $\mathbf{3}^{+}$ to the dioxidized form $\mathbf{3}^{2+}$ followed by electronic absorption spectroscopy shows that the main transition is shifted toward higher energies and is also more intense. Again, the electronic absorption spectrum does not enable us to conclude on the nature of this oxidation. Should the electronic structure of $\mathbf{3}^{2+}$ be Ru^{II}-dicyd^{0}-Ru^{II}, this transition could be assigned to a

$d\pi(Ru(II)) \rightarrow \pi^*(\ dicyd^0)$ MLCT transition. Now, supposing the electronic structure is Ru^{II}- $dicyd^{\bullet-}$-Ru^{III}, we could attribute this transition to an intervalence transition. The dioxidized form $\mathbf{3}^{2+}$ is EPR silent, which is compatible with both electronic structures. Ru^{II}-$dicyd^0$-Ru^{II} is clearly diamagnetic whereas in the case of Ru^{II}- $dicyd^{\bullet-}$-Ru^{III} the absence of signal in EPR could be interpreted by a strong antiferromagnetic coupling between the Ru(III) ion and the anion radical ligand (or between the two Ru(III) ions for Ru^{III}-$dicyd^{2-}$-Ru^{III}).

Insert Scheme 3 and Table 4

The ground state of the EPR-silent complex $\mathbf{3}^{2+}$ might, in principle, be either a closed-shell singlet or an antiferromagnetically coupled open-shell singlet. We performed the calculation assuming it was a closed-shell singlet.

The computed structural parameters of complex $\mathbf{3}^{2+}$ in its closed shell singlet state at the B3LYP level of theory are found to be in good agreement with the corresponding values obtained from the X-ray structure. The largest deviations between experimental and computed bond lengths and angles are only about 0.07 Å and 3.6° respectively.

The optimized structure shows that the geometry of the bridging ligand is intermediate between the optimized geometries of the two forms L^- and L^0 of the free ligand, but rather closer to the geometry of the radical anionic form. Another argument in favour of the oxidation of the metal is the shortening of the metal-ligand bond (g) by 0.05 Å from complex $\mathbf{3}^+$ to complex $\mathbf{3}^{2+}$. This trend may be explained on an electrostatic point of view. Assuming the oxidation from $\mathbf{3}^+$ to $\mathbf{3}^{2+}$ is based on the metal, the charge on the bridging ligand is then unchanged (1-), whereas the formal charges on the two metals increase from 2+ to 2.5+. One should then expect the attraction between the metal and the ligand to increase and the length of the metal-ligand bond to decrease. On the other hand, if the ligand was oxidized once more at this stage, its charge would change from 1- to 0 whereas the formal charges on the metals would remain the same. This should end up in a lengthening of the metal-ligand bond, which is not the case.

Examining the evolution of the atomic charges shows that the 2+ charge is distributed half on the bridging ligand (46 % to 50 %) and half on the [Ru(tpy)(thd)] moiety (50 % to 52 %), which would be in favour of a metal centered oxidation.

Regarding molecular orbitals, the LUMO of complex $\mathbf{3}^{2+}$ resembles at first sight the SOMO of $\mathbf{3}^{+}$ and the HOMO of **3** (see correlation diagram of Figure 13), suggesting that oxidation has occurred here. However the LUMO of $\mathbf{3}^{+}$ (Figure 10) exhibits a decreased contribution from the ligand (70 %) and an increased contribution from the two ruthenium atoms (18 %), showing some tendency to oxidize the metal(s). The HOMO mainly implies the ruthenium moieties, (Figure 11) with 43 % on the ruthenium atoms, 43% on the thd ligands and only 9 % on the bridging ligand. The composition of the LUMO (figure 10) does not enable us to conclude clearly as it shows that the second oxidation occurred half on the bridging ligand (40 %) and half on the [Ru(tpy)(thd)] moiety (60 %).

To sum up, the determination of the oxidation site from $\mathbf{3}^{+}$ to $\mathbf{3}^{2+}$ is not so clear as for the first oxidation, and a ruthenium-based oxidation, as we tentatively assumed from the experimental data, is possible. Note that the present calculations are valid for isolated molecules (gas phase) while the experimental study is made in solution. This could explain why experimental and theoretical results are not in complete agreement.

Insert Figures 10 and 11

Here, the X-ray structure of $\mathbf{3}^{2+}$ can give good pieces of information concerning the electronic structure. One can compare the structure of the coordinated ligand to the structure of its free dianionic form $dicyd^{2-}$ and of its free neutral form $dicyd^{0}$. It is interesting to notice that upon oxidation of $dicyd^{2-}$ to $dicyd^{0}$, the structure of the ligand changes from a benzenic form to a quinonic form : one can observe a shortening of bonds **b** (C-C) and **d** (C-N) and a lengthening of bonds **a** and **c** (C-C) (See Scheme 3, Table 4). Comparing a few bond lengths, the structure of the coordinated ligand in complex $\mathbf{3}^{2+}$ appears to be halfway between the free dianionic form $dicyd^{2-}$ and the free neutral form $dicyd^{0}$, which seems to indicate that the coordinated ligand is in its monooxidized form $dicyd^{\bullet-}$ in dinuclear complex $\mathbf{3}^{2+}$. This

structure is intermediate between the benzenic structure of the dianion dicyd^{2-} and the quinonic structure of DCNQI (dicyd^{0}) as shown for dicyd$^{\bullet-}$ salts with porphyrinatomanganese(II). [31]

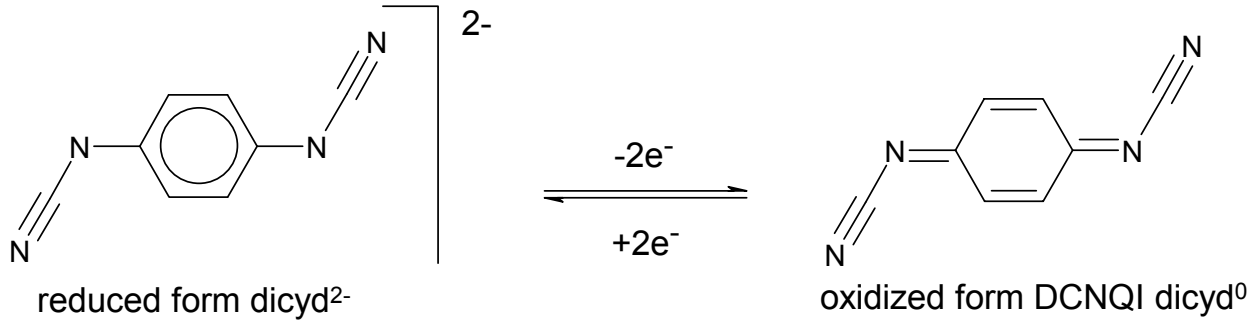

reduced form dicyd^{2-} oxidized form DCNQI dicyd^{0}

This would be a nice example of a mixed-valence system where the electronic interaction would occur through a radical anionic ligand.

3.4 The tri- and tetraoxidized forms 3^{3+} and 3^{4+}

Upon further oxidation from $\mathbf{3}^{2+}$ to $\mathbf{3}^{3+}$, the transition at 1290 nm disappears and a sharper transition appears at 1018 nm. The shape and the energy of this transition are similar to that of LMCT transitions observed for Ru(III) mononuclear complexes ; the electronic structure of $\mathbf{3}^{3+}$ would then appear to be Ru^{III}- dicyd$^{\bullet-}$-Ru^{III}. This transition could then be attributed to a π(dicyd$^{\bullet-}$)$\rightarrow$ dπ(Ru(III) LMCT transition.

The EPR of $\mathbf{3}^{3+}$ shows a broad and isotropic signal centered on g = 2.08. This is neither characteristic of a radical species (in which case the signal should be sharp and centered on 2.00) nor of a low spin Ru(III) ion (which is a rhombic system). However, assuming the electronic structure of $\mathbf{3}^{3+}$ to be Ru^{III}-dicyd$^{\bullet-}$-Ru^{III}, the EPR spectrum could be interpreted as the signal of an effective spin ½ resulting of the interaction of three highly coupled spins ½ (carried by two Ru(III) ions and the anion radical dicyd$^{\bullet-}$).

This is coherent with what can be observed during the oxidation from $\mathbf{3}^{3+}$ to $\mathbf{3}^{4+}$ followed by spectroelectrochemistry. During this step, the ligand is oxidized from dicyd$^{\bullet-}$ to dicyd^{0}, which causes the disappearance of the π(dicyd$^{\bullet-}$)$\rightarrow$ dπ(Ru(III) LMCT transition at 1018 nm.

4 General conclusion

Multiple spectroscopic, electrochemical, and spectroelectrochemical investigations have revealed the influence of the dicyanamidobenzene bridging ligand system on the intramolecular electron transfer abilities of binuclear ruthenium complexes.

We have attempted to establish the oxidation state distribution for the various accessible redox states of compound **3**, using a combination of UV-Visible-NIR and spectroelectrochemistry. Theoretical calculations at the DFT level for **3**, $\mathbf{3}^{+}$, $\mathbf{3}^{2+}$ were also helpful and are in general agreement with experimental data.

It has been shown that

- The dicyanamido ligand is a truly 'non-innocent' bridging ligand and is oxidized first.
- Then one of the Ru(II) ions is oxidized next to form a Ru^{II}- $dicyd^{\bullet-}$-Ru^{III} system which would possibly be one of the rare examples[17] of an unconventional mixed-valent system where the electronic interaction occurs through an open shell anion radical ligand and a new class of singlet species composed from metal/ligand/metal intramolecular spin-spin coupling. At the present stage it is not possible to know if the mixed valence is localized (class II) or delocalized (class III) according to Robin and Day classification.[32]
- The third oxidation produced the Ru^{III}- $dicyd^{\bullet-}$-Ru^{III} system where metal- and ligand-based spins are in strong antiferromagnetic interaction, leading to a net effective S = 1/2 resultant spin state. This would then open the possibility to study both the electro and the magnetocommunication in the same system in the near future.

One may notice that a simple electrostatic argument may be evoked to explain the order of these oxidations, once admitted that the first site of oxidation, starting from **3**, is the dicyanamido ligand. If the ligand is oxidized first, it will be difficult to oxidize it once more. The metal is thus oxidized next and then the other metal, which is farther from the first oxidized metal than the ligand. Finally the ligand is oxidized to the neutral state at the end, when there is no other choice.

The first goal of this study was to look for a mixed-valent system with a good electronic communication. The dicyanamidobenzene ligand was supposed to be well suited to mediate metal-metal interactions because of the close proximity in energy of its HOMO with the metal orbitals. By this very fact, we have found a more complicated system, full of potentiality, *ie* the capability to finely modulate the interaction between the two metals with slight modifications of the bridging ligand or of the ancillary ligands.

5 Experimental Section

5.1 Materials

All chemicals and solvents were reagent grade or better. $[Ru(tpy)Cl_3]$,[33] IpcydH,[21] $dicydH_2$,[7] $[AsPh_4]_2[dicyd]$ [7, 9] were prepared according to literature procedures. Weakly acidic Brockmann I type alumina (Aldrich) was used.

5.2 Physical Measurements

UV-visible spectra were recorded on a Shimadzu UV-3100 spectrophotometer. ^1H and ^{13}C NMR spectra were recorded on a Bruker AMX-500 in CD_2Cl_2. IR spectra of samples in KBr pellets were taken on a Perkin-Elmer 1725 FT-IR spectrophotometer. Mass spectra were recorded by the 'Service de Spectroscopie de Masse' of Paul Sabatier University using FAB (Nermag R10-R10, NBA matrix) or ES (Perkin-Elmer Sciex System API 365). Cyclic voltammograms were obtained with an Autolab system (PGSTAT 100) in dry dimethylformamide (DMF), dichloromethane (DCM) or acetonitrile (0.1 M tetrabutylammonium hexafluorophosphate, TBAH) at 25 °C with a three-electrode system consisting of platinum-disk working (1mm diameter), platinum-wire counter and saturated calomel reference electrodes. Electrochemical oxidations were performed by electrolysis with coulometry in dry DMF, dichloromethane or acetonitrile (0.1 M TBAH) at 25 °C at fixed potential with a three-electrode system consisting of platinum-net working, platinum-wire counter and saturated calomel reference electrodes. EPR experiments were performed in frozen DCM solution (100 K) with a typical concentration of $5x10^{-4}$ M on a Bruker Elexys 500 E X-band spectrometer (equiped with Bruker NMR Teslameter). Magnetisation measurements were performed using a conventional SQUID Quantum Design MPMS-5

magnetometer. This magnetometer works between 1.75 K and 300 K with a stability of temperature lower than 0.01K. The magnetic field was obtained using a superconducting magnet (max field ± 5 T) which provides a highly uniform field. Measurements were made using the reciprocating sample option (RSO), which provides a high accuracy of DC measurements (SQUID sensitivity of 10^{-7} emu). The sample holder did not give any paramagnetic signal and its diamagnetic signal was too low compared to the sample signal to give any visible contribution. Diamagnetic susceptibilities corrections for [**2**][PF6] and [**3**][PF6] were taken as -639x10^{-6} and -767x10^{-6} cm^3mol^{-1} respectively using Pascal's constant.[34]

5.3 Synthesis of complexes

Synthesis of [Ru(tpy)(thd)Cl] 1. [Ru(tpy)Cl_3] (417 mg, 0.946 mmol) was placed in solution in ethanol (200 ml). The brown suspension was degassed and the apparatus was flushed with argon and triethylamine (1.4 ml, 11 equiv.) and 2,2,6,6-tetramethyl-3,5-heptanedione (1.6 ml, 8 equiv.) were added. The mixture was heated under reflux for 2 h. The solution, which had turned dark purple, was allowed to cool down at room temperature and then evaporated to dryness. The dark residue was dissolved in dichloromethane (100 ml) and the resulting solution was filtered through celite, leaving a purple-black solid and a blue-green filtrate, which was evaporated to dryness. Ether was then added to the resulting solid, giving a suspension of a blue-green powder, which was filtered and washed with water and ether before being air dried (187 mg, 36%). ^{1}H NMR (CD_2Cl_2 δ=5.35): 8.67 (2H, ddd, 5.6 Hz, 1.5 Hz and 0.9 Hz) ; 8.14 (2H, ddd, 8.1 Hz, 1.3 Hz and 0.9 Hz) ; 8.06 (2H, d, 8.0 Hz) ; 7.79 (2H, ddd, 8.1 Hz, 7.5 Hz and 1.5 Hz) ; 7.48 (2H, ddd, 7.5 Hz, 5.6 Hz and 1.3 Hz) ; 7.43 (1H, t, 8.0 Hz) ; 5.58 (1H, s) ; 1.57 (9H,s) ; 0.45 (9H, s). ^{13}C NMR (CD_2Cl_2 δ=53.48): 195.7, 195.3, 162.0, 159.7, 151.1, 134.6, 126.2, 125.4, 121.0, 119.3, 91.0, 41.6, 40.1, 28.6, 27.5. FAB mass spectrum (DMF) m/z : 553 $[M]^+$ (calc. 553.1) ; 518 $[Ru^{II}(tpy)(thd)]^+$ (calc. 518.1) ; 370 $[Ru^{II}(tpy)Cl]^+$ (calc. 370.0). Anal. Calc. for $RuC_{26}H_{30}N_3O_2Cl$: C, 56.5, H, 5.5, N, 7.6. Found: C, 56.1, H, 5.5, N, 7.5%. CV (DCM, 0.1M TBAH, 0.1Vs^{-1}, vs SCE) $E_{1/2}(Ru^{II}/Ru^{III})$ = 0.198 V.

Synthesis of [Ru(tpy)(thd)(Ipcyd)] 2. To a dark blue solution of **1** (250 mg, 0.452 mmol) in an ethanol/water mixture (5:1, 120 ml) previously degassed was added silver hexafluorophosphate (238

mg, 0.941 mmol, 2.1 equiv.), which caused the solution to turn brown-green. The mixture was heated under reflux for 3.5 h and then allowed to cool down before being filtered through celite. IpcydH (1.15 g, 4.71 mmol, 10.4 equiv.) was added to the purple filtrate and the solution was stirred under argon at 40 °C for 66 h. At this stage, evaporation of the mixture gave a solid, which was purified by column chromatography (weakly acidic alumina, solvent: dichloromethane, eluent: dichloromethane/ethanol 99.2:0.8). The second band (dark blue) was collected, evaporated to dryness and recristallized from a mixture of dichloromethane and cyclohexane to give a dark blue powder of **2** (225 mg, 65%). ^{1}H NMR (CD_2Cl_2 δ=5.35): 8.62 (2H, ddd, 5.5 Hz, 1.5 Hz and 0.9 Hz) ; 8.15 (2H, ddd, 8.0 Hz, 1.4 Hz and 0.9 Hz) ; 8.07 (2H, d, 8.0 Hz) ; 7.86 (2H, ddd, 8.0 Hz, 7.6 Hz and 1.5 Hz) ; 7.52 (1H, t, 8.0 Hz) ; 7.50 (2H, ddd, 7.6 Hz, 5.5 Hz and 1.4 Hz) ; 7.13 (2H, d, 8.7 Hz) ; 6.09 (2H, d, 8.7 Hz) ; 5.64 (1H, s) ; 1.56 (9H, s) ; 0.49 (9H, s). ^{13}C NMR (CD_2Cl_2 δ=53.48): 196.9, 196.8, 160.9, 159.6, 153.3, 150.7, 136.9, 135.1, 126.7, 126.0, 125.8, 121.6, 121.3, 120.1, 88.9, 76.5, 41.6, 40.2, 28.7, 27.6. IR ν/cm^{-1} 2175s (NCN). ES mass spectrum (CH_3CN) m/z: 762.3 $[M + H]^+$ (calc. 762.1) ; 546.3 $[Ru(tpy)(thd)(HCN) + H]^+$ (calc. 546.2). Anal. Calc. for $RuC_{33}H_{34}N_5O_2I(H_2O)$: C, 50.9 ; H, 4.7 ; N, 9.0. Found: C, 50.7 ; H, 4.6 ; N, 8.9%. CV (DCM, 0.1M TBAH, 0.1Vs^{-1}, vs SCE) $E_{1/2}(Ru^{II}/Ru^{III})$ = 0.200 V.

Synthesis of [2][PF$_6$]. To a dark blue solution of **2** (100 mg, 0.131 mmol) in dichloromethane (50 ml) previously degassed with argon was added ferrocenium hexafluorophosphate (55 mg, 0.17 mmol, 1.3 equiv.). The solution was stirred under argon at room temperature for 45 mn and turned golden brown. The solution was filtered through celite and the filtrate was concentrated before cyclohexane was added. The obtained precipitate was filtered and washed successively with cyclohexane and ether before being air dried to yield a green powder (94 mg, 79 %). IR ν/cm^{-1} 2115s (NCN) and 843s (PF_6). ES mass spectrum (CH_3CN) m/z: positive mode: 761.3 $[M]^+$ (calc. 761.1) ; negative mode: 145.1 $[PF6]^-$ (calc. 145.0). Anal. Calc. for $RuC_{33}H_{34}N_5O_2IPF_6(C_6H_{12})_{0.2}$: C, 44.5 ; H, 4.0 ; N, 7.6. Found: C, 44.4 ; H, 3.9 ; N, 7.6%.

Synthesis of [{Ru(tpy)(thd)}$_2$(μ-dicyd)][PF$_6$] [3][PF$_6$]. To a dark blue solution of **1** (310 mg, 0.561 mmol) in an ethanol/water mixture (5:1, 120 ml) previously degassed was added silver

hexafluorophosphate (283 mg, 1.12 mmol, 2.0 equiv.) and the solution turned brown-green. The mixture was heated under reflux for 3 h and then allowed to cool down before being filtered through celite. $DicydH_2$ (45 mg, 0.28 mmol, 0.51 equiv.) was added to the purple filtrate and the solution was stirred under argon at 40 °C for 48 h. Evaporation of the mixture gave a solid, which was purified by column chromatography (weakly acidic alumina, solvent: dichloromethane, eluent: dichloromethane/ethanol 99:1). The first band (purple) was collected, evaporated to dryness and recristallized twice from a mixture of dichloromethane and cyclohexane to give a dark purple powder of **3** (109 mg, 29%). IR ν/cm^{-1} 2092s (NCN) and 845s (PF_6). ES mass spectrum (CH_3CN) m/z: 1192.6 $[M]^+$ (calc.1192.3) ; 676.5 [Ru(tpy)(thd)(dicydH)+H]$^+$ (calc. 676.2) ; 546.3 [Ru(tpy)(thd)(HCN) + H]$^+$ (calc. 546.2) ; 145.1 $[PF_6]^-$ (calc. 145.0). Anal. Calc. for $Ru_2C_{60}H_{64}N_{10}O_4PF_6$: C, 53.9 ; H, 4.8 ; N, 10.5. Found: C, 53.7 ; H, 5.0 ; N, 10.4%.

Synthesis of [{Ru(tpy)(thd)}$_2$(μ-dicyd)][PF$_6$]$_2$ [3][PF$_6$]$_2$. To a solution of [**3**][PF_6] (16.2 mg, 0.012mmol) in freshly distilled dichloromethane (10 ml) was added ferrocenium hexafluorophosphate (4.8 mg, 0.015 mmol, 1.2 equ.). The solution was stirred under argon at room temperature for 1 hour and its color turned from purple to orange pink. It was filtered through celite and the filtrate was concentrated to 5-10 ml. Cyclohexane (30 ml) was added and the obtained precipitate was filtered and washed with cyclohexane and ether to yield a dark purple powder of [**3**][PF_6]$_2$ (12.3 mg, 0.008 mmol, 69%). ES mass spectrum (CH_3CN) m/z: positive mode: 1337.9 $[M^{2+}, PF_6^-]^+$ (calc.1337.3) ; 596.2 $[M]^{2+}$ (calc. 596.2) ; negative mode: 145.3 $[PF_6]^-$ (calc. 145.0).

5.4 Crystal structure determination of [3][PF$_6$]$_2$

Dark red needles were grown by slow diffusion of cyclohexane into a dichloromethane solution of the complex. The diffraction intensities were collected on a Nonius Kappa CCD diffractometer at a temperature of 298 K, using graphite monochromatic Mo-Kα radiation (λ = 0.71073 Å) at a detector distance of 4 cm. The crystallographic cell was found by using EVAL-CCD. [35] The structure was solved using DIRDIFF [36] and refined in the maXus software package. [37] Absorption corrections were performed using SORTAV program 'Blessing 1995'. The refinement was performed anisotropically for

all the non-hydrogen atoms of the complex (SHELXL-97) [38]. The hydrogen atoms were localized by difference Fourier synthesis, recalculated and fixed at 0.97 Å, then their contributions were introduced in the calculations but not refined. 4313 reflections [$I > 2\sigma(I)$] were used for the 814 parameters and the R value dropped to 0.0665. The full experimental details, atomic parameters and the complete listing of bond lengths and angles are available as supplementary data.

5.5 Computational details

Calculations were performed with the GAMESS (General Atomic and Molecular Electronic Structure System) software.[39] Complete geometry optimizations were carried out using the density functional theory method with the conventional Becke-3-Lee-Yang-Parr (B3LYP) exchange-correlation functional.[40] Hydrogen atoms were assigned 6-31G basis set. The Stevens-Basch-Krauss-Jasien-Cundari (SBKJC) effective core potential and the corresponding valence basis set [41] were employed for all other atoms including ruthenium. Initial geometries were prepared by a molecular mechanics calculation using the universal force field developed by Rappe and Goddard, [42] in a Cerius environment. The optimized geometries are summarized in the supporting information. Representations of the molecular orbitals were obtained using Molekel. [43]

Theoretical study was conducted in order to shed light on the behavior of **3** toward oxidation, in particular with respect to the site of oxidation. The calculation was made using DFT, with a suitable pseudo-potential for Ru. In a first step, we investigated the question of geometry.

The dinuclear complex **3** possesses several geometrical degrees of freedom. Concerning the ancillary ligands, the conformation of the terpyridine ligand can be considered locked and the four tert-butyl groups on the thd ligands are in almost free rotation. Concerning the geometry of the bridging ligand, the cyanamide groups are almost linear, but two degrees of freedom can be identified on each moiety (See Figure 12) : the dihedral angle θ_1 (C_1-N_5-C_2-C_3) between the phenyl plane and the cyanamide and the angle θ_2 (N_2-Ru-N_5-C_4) corresponding to the rotation of the whole phenylcyanamide group around the Ru-N bond (like a flag).

Insert Figure 12

Preliminary work on mononuclear complex [Ru(tpy)(thd)(pcyd)] showed that the rotation θ_2 is virtually free while there is an appreciable barrier for rotation along θ_1, with energy minimum for θ_1 = 0° or 180°. (Work to be published) This was consistent with X-Ray observations on different complexes of this type, showing that the values for θ_1 were always around 0°, whereas θ_2 could adopt different values: 41°, [21] 69°, [20] 77°, [44] 116° (this work). The value of θ_1 was thus taken equal to 0° (or 180°) and the value of θ_2 was arbitrarily chosen equal to 0°.

In addition, the bridging ligand can adopt either a *syn* or an *anti* conformation, corresponding to the following combinations (θ_1 = 0° and θ'_1 = 180°) and (θ_1 = 0° and θ'_1 = 0°) respectively. X-ray structures of complexes containing the dicyanamidobenzene bridging ligand showed that these complexes usually adopt the *anti* conformation, [7, 10] which should be intuitively the more stable. We adopted this conformation for our calculations.

For the sake of comparison, we also optimized the geometry of the free bridging ligand in its dianionic ($\mathbf{L^{2-}}$), radical anionic ($\mathbf{L^{-}}$) and neutral ($\mathbf{L^{0}}$) forms (See Table 5 and scheme 3)

Orbital contours and optimized coordinates for complexes **3**, $\mathbf{3^{+}}$ and $\mathbf{3^{2+}}$ are provided in the supporting information.

Insert Table 5

Insert Table 6

The variations of atomic charges upon oxidation of the binuclear complex **3** are given in Table 6. The total and partial spin densities for $\mathbf{3^{+}}$ are given in Table 7. Finally, Figure 13 displays the correlation diagram of molecular orbitals for the series of ligands and complexes obtained upon the first two oxidations : $\mathbf{L^{2-} \rightarrow L^{-} \rightarrow L^{0}}$ and $\mathbf{3 \rightarrow 3^{+} \rightarrow 3^{2+}}$. To test the validity of the molecular orbital method, we have used the orbital energies to predict the transition energies. Although we have used here normal DFT (and not TD-DFT), there is usually a good correlation between experimental transition energies and orbital energy differences. [45]

Insert Table 7

For the $\mathbf{L^{2-} \rightarrow L^{-} \rightarrow L^{0}}$ series, the observed and calculated wavelengths are given on Table 8.

In the energy correlation diagram of Figure 13 are reported the relative energy positions of the frontier orbitals of $\mathbf{L}^{2-}$, $\mathbf{L}^{\cdot-}$ and $\mathbf{L}^{0}$ species and of the complexes $\mathbf{3}^{0}$, $\mathbf{3}^{1+}$ and $\mathbf{3}^{2+}$. For the isolated bridging ligand "dicyd", the occupied and unoccupied frontier molecular orbitals are stabilized upon oxidation. The stabilization energy value is calculated to be equal to 5 eV for $\mathbf{L}^{2-}/\mathbf{L}^{\cdot-}$and equal to 4 eV for $\mathbf{L}^{\cdot-}/\mathbf{L}^{0}$. Upon oxidation, the HOMO-LUMO energy gap varied for each degree of oxidation as follow: $\Delta E_{HOMO\text{-}LUMO}$ = 3.8 eV for $\mathbf{L}^{2-}$, 4.23 (α) 2.6 (β) eV for $\mathbf{L}^{\cdot-}$ and 3 eV for $\mathbf{L}^{0}$.

In the open electron shell $\mathbf{L}^{\cdot-}$, the spin polarization energy value between the highest α-spin and β-spin occupied molecular orbitals is equal to 3.5 eV, This polarization is attenuated when $\mathbf{L}^{\cdot-}$ is inserted in the complex 3^{+}.

Insert Table 8

In Table 9 are reported the wave lengths (in nm) associated to the lowest energy electron transitions calculated (from the MO energies) for the three oxidation forms of the isolated bridging ligand in comparison with the experimental UV-Vis absorption spectra band locations. The calculated values are globally in agreement with the UV-Vis experimental determinations.

For the complexes, a μ-dicyd orbital is always found between a set of d_{π}-thd levels and a set of d_{π^*}-tpy levels. This peculiar orbital is the HOMO in the neutral complex **3**, a single occupied and spin polarized in $\mathbf{3}^{+}$ and it is the LUMO in $\mathbf{3}^{2+}$ (See Figure 13).

Insert Figure 13

Insert Table 9

In Table 9 are summarized the calculated values of the wave lengths associated to the lowest energy electron transitions for **3**, $\mathbf{3}^{+}$ and $\mathbf{3}^{2+}$ complexes in comparison with the experimental UV-Vis absorption spectra. For $\mathbf{3}^{2+}$ the UV-Vis absorption bands at 472 and at 1290 nm can be attributed respectively to the allowed HOMO → LUMO+1 ((d_{π}-thd) → (d_{π^*}-tpy)) and HOMO → LUMO ((d_{π}-thd) → (μ-dicyd)) transitions. For $\mathbf{3}^{+}$ many electron transitions ((μ-dicyd) → (d_{π^*}-tpy)), ((d_{π}-thd) → (μ-dicyd)) and ((d_{π}-thd) → (d_{π^*}-tpy)) can contribute to the absorption band located at 530 nm. For **3** the experimental

absorption band at 588 nm can be assigned to the HOMO-1 → LUMO ((d_{π}-thd) → ($d_{\pi*}$-tpy)) electron transition. The lowest two electron transitions are calculated to be at 1582 nm (HOMO → LUMO) and at 1493 (HOMO → LUMO+1), the laters are not observed in the experimental UV-Vis spectrum. For the complex $\mathbf{3}^{+}$, three calculated transitions at 527, 473 and 574 nm can be convoluted to be assigned to the experimental band observed at 530 nm. However, the observed band at 1366 nm can not be assigned from our calculations.

Acknowledgment.

The authors thank CNRS and MENRS (M.F.) for financial support, Alain Mari (LCC, Toulouse) for EPR measurements, Yannick Coppel (LCC, Toulouse) for NMR experiments, Stéphane Ami (CEMES, Toulouse), Jean-Louis Heully and Fabienne Alary (IRSAMC, Toulouse) for technical help and helpful advices on theoretical calculations. Sylvain Bertaina and Bernard Barbara (Laboratoire Louis Néel, Grenoble) are greatly acknowledged for magnetic susceptibility measurements.

Supporting Information Available.

X-ray crystallographic files in CIF format for the structure determination of [**3**][PF_6]$_2$, CCDC 263306. These data can be obtained free of charge via www.ccdc.cam.ac.uk/data_request/cif , by emailing data_request@ccdc.cam.ac.uk , or by contacting The Cambridge Crystallographic Data Centre, 12, Union Road, Cambridge CB2 1EZ, UK ; fax: +44 1223 336033.". Figure S1: Differential pulse voltammogram of complex [**3**][PF_6], rotating platinum disk working electrode, 0.1 M TBAH in DCM, scan rate 0.1 V/s. Figure S2: Stepwise spectroelectrochemical oxidation of [$AsPh_4$]$_2$[dicyd] in DCM, 0.1M TBAH (electrolysis at 0.00 V vs SCE). Figure S3: Stepwise spectroelectrochemical reduction of [**3**][PF_6] in DCM, 0.1M TBAH (electrolysis at -0.50 V vs SCE). Figure S4: Stepwise spectroelectrochemical oxidation of [**3**][PF_6] ($\mathbf{3}^{+} \rightarrow \mathbf{3}^{2+}$) in DCM, 0.1M TBAH (electrolysis at 0.46 V vs SCE). Figure S5: Stepwise spectroelectrochemical oxidation of [**3**][PF_6] ($\mathbf{3}^{2+} \rightarrow \mathbf{3}^{3+}$) in DCM, 0.1M TBAH (electrolysis at 0.85 V vs SCE). Figure S6: Stepwise spectroelectrochemical oxidation of [**3**][PF_6] ($\mathbf{3}^{3+} \rightarrow \mathbf{3}^{4+}$) in DCM, 0.1M TBAH (electrolysis at 1.30 V vs SCE). Figure S7: Experimental (top) EPR spectrum of [**2**][PF_6] in frozen CH_2Cl_2 (100 K) and simulated (bottom). Figure S8: ORTEP drawing of the two conformers A and B of the dinuclear complex [**3**][PF_6]$_2$ - Selected bond lengths and bond angles from the X-Ray structure of [**3**][PF_6]$_2$. - Optimized coordinates and electronic total energy for ligands $dicyd^{2-}$, $dicyd^{-}$, $dicyd^{0}$, and complexes **3**, $\mathbf{3}^{1+}$, $\mathbf{3}^{2+}$ in their ground state and selected Molecular Orbital contours for $dicyd^{2-}$, $dicyd^{-}$, $dicyd^{0}$ and **3**, $\mathbf{3}^{1+}$, $\mathbf{3}^{2+}$ at the B3LYP level.

References:

1. McCleverty, J. A.; Ward, M. D. *Acc. Chem. Res.* **1998,** 31, (12), 842.
2. Kaim, W.; Klein, A.; Gloeckle, M. *Acc. Chem. Res.* **2000,** 33, (11), 755.
3. Solomon, E. I.; Brunold, T. C.; Davis, M. I.; Kemsley, J. N.; Lee, S. K.; Lehnert, N.; Neese, F.; Skulan, A. J.; Yang, Y. S.; Zhou, J. *Chem. Rev.* **2000,** 100, 235.
4. Launay, J.-P. *Chem. Soc. Rev.* **2001,** 30, 386; Launay, J.-P.; Coudret, C., Wires Based on Metal Complexes. In *Electron Transfer in Chemistry*, Balzani, V., Ed. Wiley-VCH: Weinheim, 2001; Vol. 5, pp 3; Ward, M. D. *Chem. Soc. Rev.* **1995,** 24, (2), 121; Paul, F.; Lapinte, C. *Coord. Chem. Rev.* **1998,** 178-180, 431; Low, P. J. *Dalton Trans.* **2005**, 2821.
5. Brunschwig, B. S.; Sutin, N. *Coord. Chem. Rev.* **1999,** 187, 233.
6. Kaim, W.; Kasack, V. *Inorg. Chem.* **1990,** 29, (23), 4696.
7. Aquino, M. A. S.; Lee, F. L.; Gabe, E. J.; Bensimon, C.; Greedan, J. E.; Crutchley, R. J. *J. Am. Chem. Soc.* **1992,** 114, (13), 5130.
8. Crutchley, R. J. *Adv. Inorg. Chem.* **1994,** 41, 273; Crutchley, R. J. *Comprehensive Coordination Chemistry II* **2004,** 2, 785.
9. Rezvani, A. R.; Evans, C. E. B.; Crutchley, R. J. *Inorg. Chem.* **1995,** 34, (18), 4600.
10. Evans, C. E. B.; Yap, G. P. A.; Crutchley, R. J. *Inorg. Chem.* **1998,** 37, (24), 6161.
11. Evans, C. E. B.; Naklicki, M. L.; Rezvani, A. R.; White, C. A.; Kondratiev, V. V.; Crutchley, R. J. *J. Am. Chem. Soc.* **1998,** 120, (50), 13096.
12. Naklicki, M. L.; Crutchley, R. J. *Inorg. Chim. Acta* **1994,** 225, (1-2), 123.
13. Rezvani, A. R.; Bensimon, C.; Cromp, B.; Reber, C.; Greedan, J. E.; Kondratiev, V. V.; Crutchley, R. J. *Inorg. Chem.* **1997,** 36, (15), 3322.
14. Ward, M. D.; McCleverty, J. A. *J. Chem. Soc. Dalton Trans.* **2002**, (3), 275.
15. Bayly, S.; McCleverty, J. A.; Ward, M. D.; Gatteschi, D.; Totti, F. *Inorg. Chem.* **2000,** 39, (6), 1288; Bayly, S. R.; Humphrey, E. R.; de Chair, H.; Paredes, C. G.; Bell, Z. R.; Jeffery, J. C.; McCleverty, J. A.; Ward, M. D.; Totti, F.; Gatteschi, D.; Courric, S.; Steele, B. R.; Screttas, C. G. *J. Chem. Soc. Dalton Trans.* **2001**, (9), 1401; Chakraborty, S.; Laye, R. H.; Paul, R. L.; Gonnade, R. G.; Puranik, V. G.; Ward, M. D.; Lahiri, G. K. *J. Chem. Soc. Dalton Trans.* **2002**, (6), 1172; Chanda, N.; Laye, R. H.; Chakraborty, S.; Paul, R. L.; Jeffery, J. C.; Ward, M. D.; Lahiri, G. K. *J. Chem. Soc. Dalton Trans.* **2002**, (18), 3496; Meacham, A. P.; Druce, K. L.; Bell, Z. R.; Ward, M. D.; Keister, J. B.; Lever, A. B. P. *Inorg. Chem.* **2003,** 42, (24), 7887; Chanda, N.; Sarkar, B.; Fiedler, J.; Kaim, W.; Lahiri, G. K. *Dalton Trans.* **2003**, (18), 3550; Frantz, S.; Reinhardt, R.; Greulich, S.; Wanner, M.; Fiedler, J.; Duboc-Toia, C.; Kaim, W. *Dalton Trans.* **2003**, (17), 3370; Maurer, J.; Winter, R. F.; Sarkar, B.; Fiedler, J.; Zalis, S. *Chem. Comm.* **2004**, (17), 1900; Patra, S.; Sarkar, B.; Ghumaan, S.; Fiedler, J.; Kaim, W.; Lahiri, G. K. *Inorg. Chem.* **2004,** 43, (19), 6108; Patra, S.; Sarkar, B.; Ghumaan, S.; Fiedler, J.; Zalis, S.; Kaim, W.; Lahiri, G. K. *Dalton Trans.* **2004**, (5), 750; Ghumaan, S.; Sarkar, B.; Patra, S.; Parimal, K.; van Slageren, J.; Fiedler, J.; Kaim, W.; Lahiri, G. K. *Dalton Trans.* **2005**, (4), 706; Kar, S.; Sarkar, B.; Ghumaan, S.; Janardanan, D.; van Slageren, J.; Fiedler, J.; Puranik, V. G.; Sunoj, R. B.; Kaim, W.; Lahiri, G. K. *Chem. Eur. J.* **2005,** 11, (17), 4901; Kar, S.; Sarkar, B.; Ghumaan, S.; Roy, D.; Urbanos, F. A.; Fiedler, J.; Sunoj, R. B.; Jimenez-Aparicio, R.; Kaim, W.; Lahiri, G. K. *Inorg. Chem.* **2005,** 44, (24), 8715; Heilmann, M.; Frantz, S.; Kaim, W.; Fiedler, J.; Duboc, C. *Inorg. Chim. Acta* **2006,** 359, (3), 821; Patra, S.; Sarkar, B.; Maji, S.; Fiedler, J.; Urbanos, F. A.; Jimenez-Aparicio, R.; Kaim, W.; Lahiri, G. K. *Chem. Eur. J.* **2006,** 12, (2), 489.
16. Kasack, V.; Kaim, W.; Binder, H.; Jordanov, J.; Roth, E. *Inorg. Chem.* **1995,** 34, (7), 1924.
17. Sarkar, B.; Patra, S.; Fiedler, J.; Sunoj, R. B.; Janardanan, D.; Mobin, S. M.; Niemeyer, M.; Lahiri, G. K.; Kaim, W. *Angew. Chem., Int. Ed.* **2005,** 44, (35), 5655.
18. Klein, A.; Lavastre, O.; Fiedler, J. *Organometallics* **2006,** 25, (3), 635.
19. Dudd, L.; Hart, M.; Ring, D.; Sondaz, E.; Bonvoisin, J.; Coppel, Y. *Inorg. Chem. Comm.* **2003,** 6, (11), 1400; Slattery, S. J.; Bare, W. D.; Jameson, D. L.; Goldsby, K. A. *J. Chem. Soc., Dalton Trans.* **1999**, 1347.

20. Fabre, M. A.; Jaud, J.; Bonvoisin, J. J. *Inorg. Chim. Acta* **2005,** 358, (7), 2384.
21. Sondaz, E.; Gourdon, A.; Launay, J.-P.; Bonvoisin, J. *Inorg. Chim. Acta* **2001,** 316, 79.
22. Griffith, J. S., *The Theory of Transition-Metal Ions*. Cambridge University Press ed.; London, 1961; p 363; Rieger, P. H. *Coord. Chem. Rev.* **1994,** 135-136, 203.
23. Sondaz, E. Synthesis and Characterizaton of Cyanamide-Ruthenium complexes. PhD thesis, Université Paul Sabatier-Toulouse III, Toulouse, 2001.
24. Kaim, W.; Ernst, S.; Kasack, V. *J. Am. Chem. Soc.* **1990,** 112, (1), 173.
25. Gerson, F.; Gesheidt, G.; Möckel, R.; Aumüller, A.; Erk, P.; Siegfried, H. *Helv. Chim. Acta* **1988,** 71, 1665.
26. Mori, T.; Inokuchi, H.; Kobayashi, A.; Kato, R.; Kobayashi, H. *Phys. Rev. B* **1988,** 38, 5913; Sakurai, T.; Nakagawa, N.; Okubo, S.; Ohta, H.; Kanoda, K.; Hiraki, K. *J. Phys. Soc. Jpn.* **2001,** 70, (6), 1794.
27. O'Connor, C. J. *Prog. Inorg. Chem.* **1982,** 29, 203.
28. Figgis, B. N.; Lewis, J.; Mabbs, F. E.; Webb, G. A. *J. Chem. Soc. (A)* **1966**, 422.
29. Stebler, A.; Ammeter, J. H.; Furholz, U.; Ludi, A. *Inorg. Chem.* **1984,** 23, 2764.
30. Kaim, W. *Coord. Chem. Rev.* **1987,** 76, 187; Bhattacharya, S.; Gupta, P.; Basuli, F. *Inorg. Chem.* **2002,** 41, 5810; Chaudhuri, P.; Verani, C. N.; Bill, E.; Bothe, E.; Weyhermueller, T.; Wieghardt, K. *J. Am. Chem. Soc.* **2001,** 123, (10), 2213; Herebian, D.; Wieghardt, K. E.; Neese, F. *J. Am. Chem. Soc.* **2003,** 125, (36), 10997; Herebian, D.; Bothe, E.; Neese, F.; Weyhermueller, T.; Wieghardt, K. *J. Am. Chem. Soc.* **2003,** 125, (30), 9116.
31. Sugiura, K.; Mikami, S.; Johnson, M. T.; Raebiger, J. W.; Miller, J. S.; Iwasaki, K.; Okada, Y.; Hino, S.; Sakata, Y. *J. Mater. Chem.* **2001,** 11, 2152.
32. Robin, M. B.; Day, P. *Adv. Inorg. Chem. Radiochem.* **1967,** 10, 247.
33. Sullivan, B. P.; Calvert, J. M.; Meyer, T. J. *Inorg. Chem.* **1980,** 34, 1404.
34. Mabbs, F. E.; Machin, D. J., *Magnetism and Transition Metal Complexes*. Chapman and Hall ed.; London, 1973.
35. Duisenberg, A. J. M. Reflections on Area Detectors. Utrecht, 1998.
36. Beurskens, P. T.; Beurskens, G.; de Gelder, R.; Garcia-Granda, S.; Gould, R. O.; Israel, R.; Smits, J. M. M. *The DIRDIF-99 program system*, University of Nijmegen, The Netherlands, 1999.
37. Mackay, S.; Gilmore, C. J.; Edwards, C.; Stewart, N.; Shankland, K., maXus Computer Program for the Solution and Refinement of Crystal Structures. In Nonius, The Netherlands, MacScience: Japan & the University of Glasgow, 1999.
38. Sheldrick, G. M. *Program for the Refinement of Crystal Structures. University of Göttingen, Germany.* **1997**.
39. Schmidt, M. W.; Balbridge, K. K.; Boatz, J. A.; Elbert, S. T.; Gordon, M. S.; Jensen, J. H.; Koseki, K.; Matsumata, N.; Nguyen, K. A.; Su, S.; Windus, T. L.; Depuis, M.; Montgomery, J. A. *J. Comput. Chem.* **1993,** 14, 1347.
40. Becke, A. D. *J. Chem. Phys.* **1993,** 98, 5648; Lee, C.; Yang, W.; Parr, R. G. *Phys. Rev.* **1988,** B37, 785.
41. Cundari, T. R.; Stevens, W. J. *J. Chem. Phys.* **1993,** 98, (7), 5555; Stevens, W. J.; Basch, H.; Krauss, M. *J. Chem Phys.* **1984,** 81, (12), 6026; Stevens, W. J.; Krauss, M. J.; Basch, H.; Jasien, P. G. *Can. J. Chem.* **1992,** 70, (2), 612.
42. Rappé, A. K.; Goddard, W. A. *J. Phys. Chem.* **1991,** 95, 3358.
43. Flükiger, P.; Lüthi, H. P.; Portmann, S.; Weber, J. *Molekel*, 4.3; Manno (Switzerland), 2000-2002; Portmann, S.; Lüthi, H. P. *Chimia* **2000,** 54, 776.
44. Sondaz, E.; Jaud, J.; Launay, J. P.; Bonvoisin, J. *Eur. J. Inorg. Chem.* **2002**, (8), 1924.
45. Guirado, G.; Coudret, C.; Hliwa, M.; Launay, J.-P. *Journal of Physical Chemistry B* **2005,** 109, (37), 17445.
46. Kato, R.; Kobayashi, H.; Kobayashi, A. *J. Am. Chem. Soc.* **1989,** 111, 5224.
47. Aquino, M. A. S.; Crutchley, R. J.; Lee, F. L.; Gabe, E. J.; Bensimon, C. *Acta Crystallographica, Section C: Crystal Structure Communications* **1993,** C49, (8), 1543.

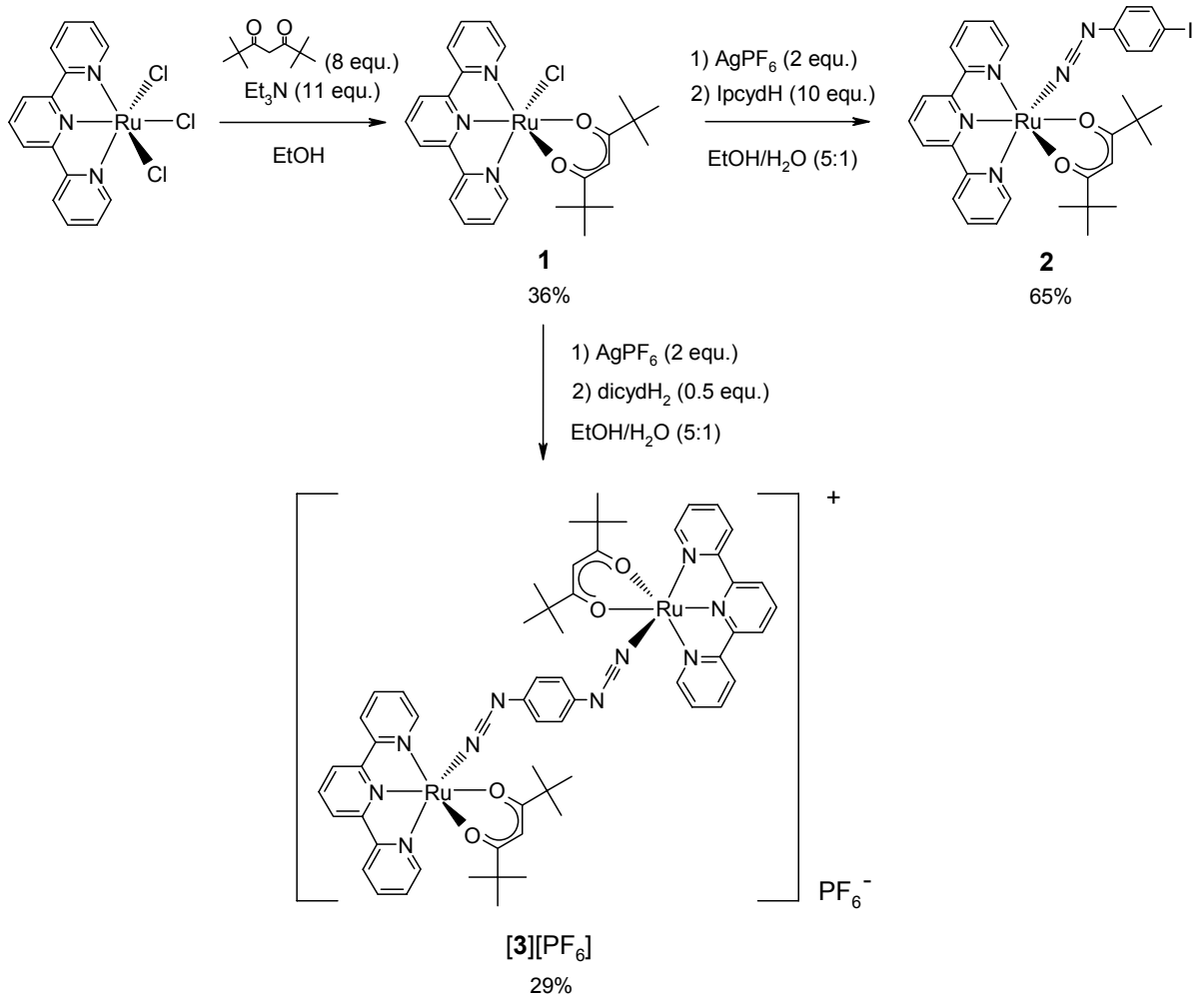

Scheme 1. Synthesis of complexes **1**, **2** and **3**.

$[Ru^{II}(\mu\text{-dicyd}^{2-})Ru^{II}]$ **3**

$+ e^-$ ⇅ $- e^-$

$[Ru^{II}(\mu\text{-dicyd}^{2-})Ru^{III}] \longleftrightarrow [Ru^{II}(\mu\text{-dicyd}^{\bullet -})Ru^{II}]$ $\mathbf{3}^{+}$

$+ e^-$ ⇅ $- e^-$

$[Ru^{III}(\mu\text{-dicyd}^{2-})Ru^{III}] \longleftrightarrow [Ru^{II}(\mu\text{-dicyd}^{\bullet -})Ru^{III}] \longleftrightarrow [Ru^{II}(\mu\text{-dicyd}^{0})Ru^{II}]$ $\mathbf{3}^{2+}$

$+ e^-$ ⇅ $- e^-$

$[Ru^{III}(\mu\text{-dicyd}^{\bullet -})Ru^{III}] \longleftrightarrow [Ru^{II}(\mu\text{-dicyd}^{0})Ru^{III}]$ $\mathbf{3}^{3+}$

$+ e^-$ ⇅ $- e^-$

$[Ru^{III}(\mu\text{-dicyd}^{0})Ru^{III}]$ $\mathbf{3}^{4+}$

Scheme 2. Various electronic structures which may be used to describe the oxidation of compound **3.**

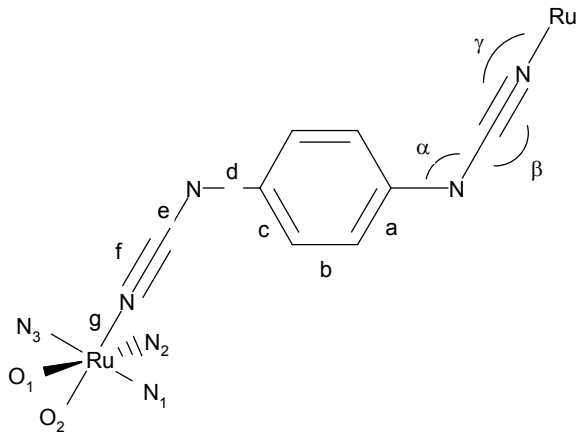

Scheme 3. Pertinent bond lengths and angles.

Table 1. Electrochemical data, 0.1M TBAH, 0.1 V/s, versus SCE.

Species	E1	E2	E3	E4	Ref
$[\{Ru(NH_3)_5\}_2(\mu\text{-dicyd})][PF_6]_4$[a]	-0.420	-0.134	0.565	0.997	12
$[\{Ru(NH_3)_4(py)\}_2(\mu\text{-dicyd})][PF_6]_4$[a]	-0.280	0.085	0.700	1.075	13
$[\{Ru(NH_3)_3(bpy)\}_2(\mu\text{-dicyd})][ClO_4]_4$[a]	-0.150	0.262	0.846	1.099	10
$[\{Ru(tpy)(bpy)\}_2(\mu\text{-dicyd})][PF_6]_2$[b]	-0.015	0.425	-	-	9
[**3**][PF_6][b]	-0.098	0.337	0.762	-	This work
[**3**][PF_6][a]	-0.145	0.224	0.658	0.924	This work
[**3**][PF_6][c]	-0.234	0.215	0.713	0.991	This work

[a] In CH_3CN, [b] In DMF, [c] in DCM.

Table 2. UV-Vis-near IR absorption data of the investigated compounds in DCM,

Species	Absorption bands, λ in nm (ε × 10^{-3} in $M^{-1}.cm^{-1}$)							
1	281(28)	319(21)	407(8.1)		573(5.6)	666(4.5)		
1^{+}	280(22)	309(18)	383(4.5)		590(1.8)			
2	281(40)	307(31)			574(5.5)			
2^{+}	265(38)	309(21)					1005(11)	
3	276(81)	314(66)			588(12)			
3^{1+}	276(73)	314(57)	380(36)	530(14)				1366(25)
3^{2+}	274(77)	312(67)		472(13)				1290(54)
3^{3+}	274(69)	314(58)		436(11)	610(12)			1018(50)
3^{4+}	280(78)	318(66)			606(12)			
$dicyd^{2-}$	265(6.4) 272(7.4)	294(13.6)						
$dicyd^{\cdot-}$	265(7.5) 272(7.7)	293(8.6)	362(4.1)		573(1.6)	620(3.0) 685(3.5)		
$dicyd^{0}$	265(8.7) 272(7.6)							

Table 3. Crystallographic Data and Refinement Parameters for [**3**][PF_6]$_2$.

Formula	$C_{60}H_{64}F_{12}N_{10}O_4P_2Ru_2$
Crystal System	Monoclinic
Fw (g mol^{-1})	1481.3
Space Group	C2/c
a, Å	27.246(2)
b, Å	30.008(2)
c, Å	20.150(2)
β, °	107.960(9)
V, Å^3	15672(2)
Z	8
μ(MoKα), (mm^{-1})	0.499
ρcalcd, (g cm^{-3})	1.256
2θ max (°)	28
Total number of reflections	17767
Number of unique reflections with I>2σ(I)	4313
Absorption correction	multi-scan
$T_{min/max}$	0.615/0.917
R_f[a]	0.0665
R_w[b]	0.174
Goodness-of-fit	0.902

[a] $R_f = \Sigma \, || Fo| - |Fc|| \, / \, \Sigma \, |Fo|$

[b] $Rw = (\Sigma \, w| Fo| - |Fc|)^2 \, / \, \Sigma \, w|Fo|^2)^{1/2}$

Table 4. Experimental data for Selective bond lengths and angles**.**

Species	DCNQI	$[AsPh_4]_2$ [dicyd]	3^{2+} (A)	3^{2+} (B)	a	b	c	d
a/Å	1.446(2)	1.398 (8)	1.410 (13)	1.402 (12)	1.406 (20)	1.440 (14) – 1.444 (14)	1.435 (6)	1.437 (3)
b/Å	1.336(2)	1.385 (9)	1.359 (13)	1.348 (12)	1.386 (20)	1.348 (14) – 1.355 (14)	1.352 (5)	1.364 (3)
c/Å	1.450 (2)	1.399 (9)	1.396 (14)	1.418 (11)	1.386 (20)	1.426 (14) – 1.426 (14)	1.428 (6)	1.411 (3)
d/Å	1.303 (2)	1.388 (8)	1.335 (12)	1.350 (10)	1.376 (17)	1.331 (12) – 1.335 (13)	1.359 (5)	1.350 (3)
e/Å	1.334 (2)	1.299 (10)	1.280 (12)	1.287 (10)	1.298 (19)	1.309 (14) – 1.316 (14)	1.309 (6)	1.306 (3)
f/Å	1.150 (2)	1.172 (10)	1.152 (11)	1.154 (10)	1.151 (19)	1.162 (13) – 1.172 (12)	1.163 (6)	1.156 (3)
g/Å	-	-	1.966 (6)	1.969 (6)	1.938 (11)	1.978 (8) – 1.977 (9)	2.261 (4)	2.249 (2)
α/°	119.5 (2)	118.7 (5)	124.4 (8)	124.0 (7)	119.7 (12)	121.3 (9) – 122.6 (9)	-	-
β/°	172.8 (2)	174.1 (6)	173.9 (10)	173.2 (8)	171.5 (15)	169.2 (10) – 173.9 (11)	173.1 (4)	175.9 (2)
γ/°	-	-	174.0 (7)	173.3 (6)	175.1 (10)	174.1 (8) – 178.1 (8)	158.4 (4)	150.7 (2)
T (K)	-	295	298	298	295	298	-	223
ref	46	47	This work	This work	7	10	31	31

a : $[\{Ru(NH_3)_5\}_2(\mu\text{-dicyd})][TsO]_4$ (conformer A).

b : $[\{$*mer*-$Ru(bpy)(NH_3)_3\}_2(\mu\text{-dicyd})][ClO_4]_4$ (not centrosymmetric).

c : $[Mn^{III}TMesP]^+[DMeDCNQI]^{\cdot-}$ = *meso*-tetrakis(2,4,6-trimethylphenyl)porphyrinatomanganese (III) 2,5-dimethyl-*N,N'*-dicyanoquinone diimine.

d : $[Mn^{III}TMesP]^+[DMeODCNQI]^{\cdot-}$ = *meso*-tetrakis(2,4,6-trimethoxyphenyl)porphyrinatomanga-nese (III) 2,5-dimethyl-*N,N'*-dicyanoquinone diimine.

Table 5. Experimental and calculated selected bond lengths (Å) and angles (°).

Species	$\mathbf{L}^{2-}$	$\mathbf{L}^{\cdot-}$	$\mathbf{L}^{0}$	$\mathbf{3}^{0}$	$\mathbf{3}^{+}$	$\mathbf{3}^{2+}$ exp. (form A)	$\mathbf{3}^{2+}$ exp. (form B)	$\mathbf{3}^{2+}$ (singlet)
a	1.440	1.453	1.481	1.432	1.449	1.410 (13)	1.402 (12)	1.461
b	1.425	1.403	1.380	1.418	1.403	1.359 (13)	1.348 (12)	1.392
c	1.443	1.458	1.484	1.439	1.454	1.396 (14)	1.418 (11)	1.466
d	1.423	1.382	1.336	1.420	1.385	1.335 (12)	1.350 (10)	1.361
e	1.323	1.336	1.351	1.290	1.313	1.280 (12)	1.287 (10)	1.311
f	1.226	1.212	1.201	1.208	1.197	1.152 (11)	1.154 (10)	1.198
g	-	-	-	2.041	2.053	1.966 (6)	1.969 (6)	2.001
Ru-N_1	-	-	-	2.097	2.106	2.099 (7)	2.069 (6)	2.121
Ru-N_2	-	-	-	1.964	1.974	1.977 (6)	1.946 (6)	1.988
Ru-N_3	-	-	-	2.097	2.106	2.062 (6)	2.051 (7)	2.121
Ru-O_1	-	-	-	2.118	2.108	2.053 (5)	2.057 (5)	2.099
Ru-O_2	-	-	-	2.095	2.083	2.024 (5)	2.039 (5)	2.054
α	121.9	122.1	123.0	123.4	123.1	124.4 (8)	124.0 (7)	125.2
β	173.2	172.7	172.3	174.5	173.8	173.9 (10)	173.2 (8)	173.1
γ	-	-	-	171.6	171.5	174.0 (7)	173.3 (6)	170.4

Table 6. Variation of atomic charges upon oxidation of the complex (calculated from Mulliken and Lowdin population analyses).

fragment	Ru_1	Ru_2	dicyd	tpy_1	tpy_2	thd_1	thd_2
ΔQ (0 → 1+) (Mulliken)	0.01	0.01	0.53	0.14	0.14	0.08	0.08
ΔQ (0 → 1+) (Lowdin)	-0.01	-0.01	0.59	0.14	0.14	0.07	0.07
ΔQ (1+ → 2+) (Mulliken)	-0.02	-0.02	0.40	0.19	0.19	0.13	0.13
ΔQ (1+ → 2+) (Lowdin)	0.03	0.03	0.42	0.16	0.16	0.11	0.11
ΔQ (0 → 2+) (Mulliken)	-0.01	-0.01	0.93	0.34	0.34	0.21	0.21
ΔQ (0 → 2+) (Lowdin)	0.02	0.02	1.01	0.30	0.30	0.18	0.18

Table 7. Total and SOMO spin densities ($\rho_{\alpha-\beta}$ and ρ_{SOMO}) for complex $\mathbf{3}^{+}$.[a]

fragment	Ru_1	Ru_2	dicyd	tpy_1	tpy_2	thd_1	thd_2
$\rho_{\alpha-\beta}$ (Mulliken)	0.05	0.05	0.92	0.00	0.00	0.00	0.00
$\rho_{\alpha-\beta}$ (Lowdin)	0.06	0.06	0.90	0.00	0.00	0.00	0.00
ρ_{SOMO} (Mulliken)	0.09	0.09	0.74	0.02	0.02	0.02	0.02

[a]Spin densities broken down into fragment contributions from metal and ligands.

Table 8. Calculated wavelengths associated to electron transitions between frontier molecular orbitals in comparison with the UV-Vis spectra, for $\mathbf{L}^{2-}$, $\mathbf{L}^{\cdot-}$ and $\mathbf{L}^{0}$ species.

λ (nm)	Experimental	homo-1→lumo	homo→lumo	homo→lumo+1
$\mathbf{L}^{2-}$	265-272-294	233	325	-
$\mathbf{L}^{\cdot-}$	265-272-293 362-573-620-680	(α-spin) 205 (β-spin) 390	293 547	- 400
$\mathbf{L}^{0}$	265-272	359	412	206

Table 9. Calculated wavelengths associated to frontier molecular orbitals electron transitions in comparison with the UV-Vis spectra, for $\mathbf{3}^{0}$, $\mathbf{3}^{+}$ and $\mathbf{3}^{2+}$ species.

λ (nm)	Experimental	homo-1→lumo	homo→lumo	homo→lumo+1
3	588	603	1582	1493
$\mathbf{3}^{+}$	530-1366	(α-spin) 592 (β-spin) 700	473 609	574 517
$\mathbf{3}^{2+}$	472-1290	1004	1241	483

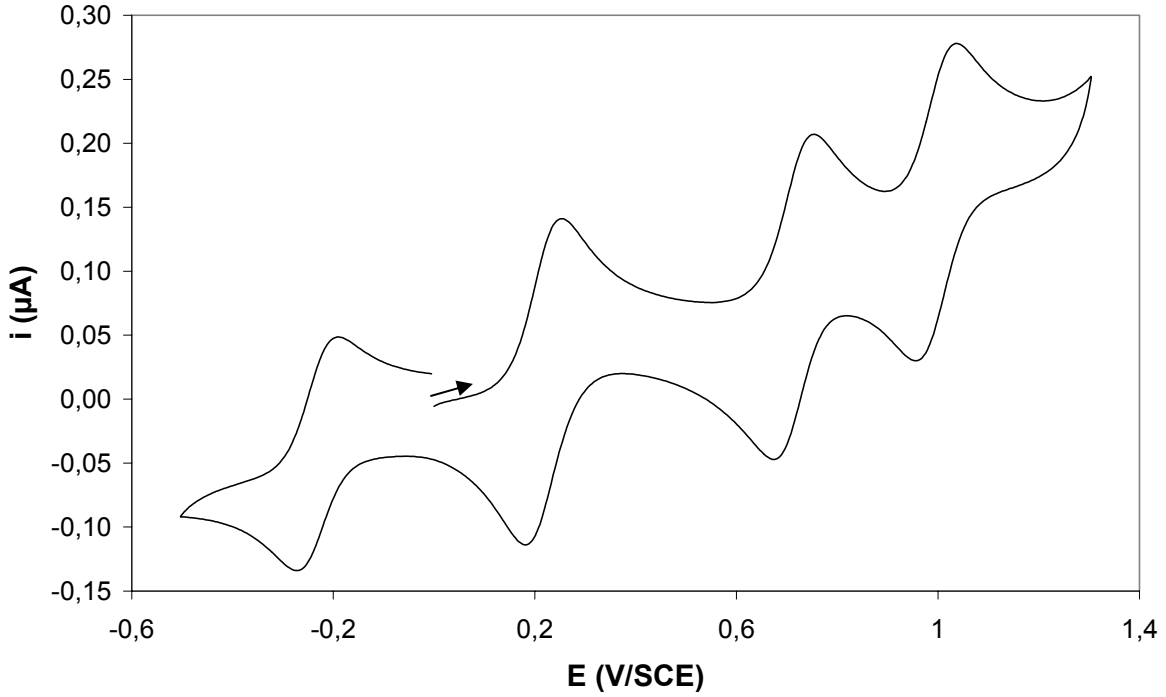

Figure 1. CV of complex [**3**][PF_6], platinum disk working electrode, 0.1 M TBAH in DCM, scan rate 0.1 V/s [Scan Range : 0.0 → +1.3 → -0.5 → 0.0V].

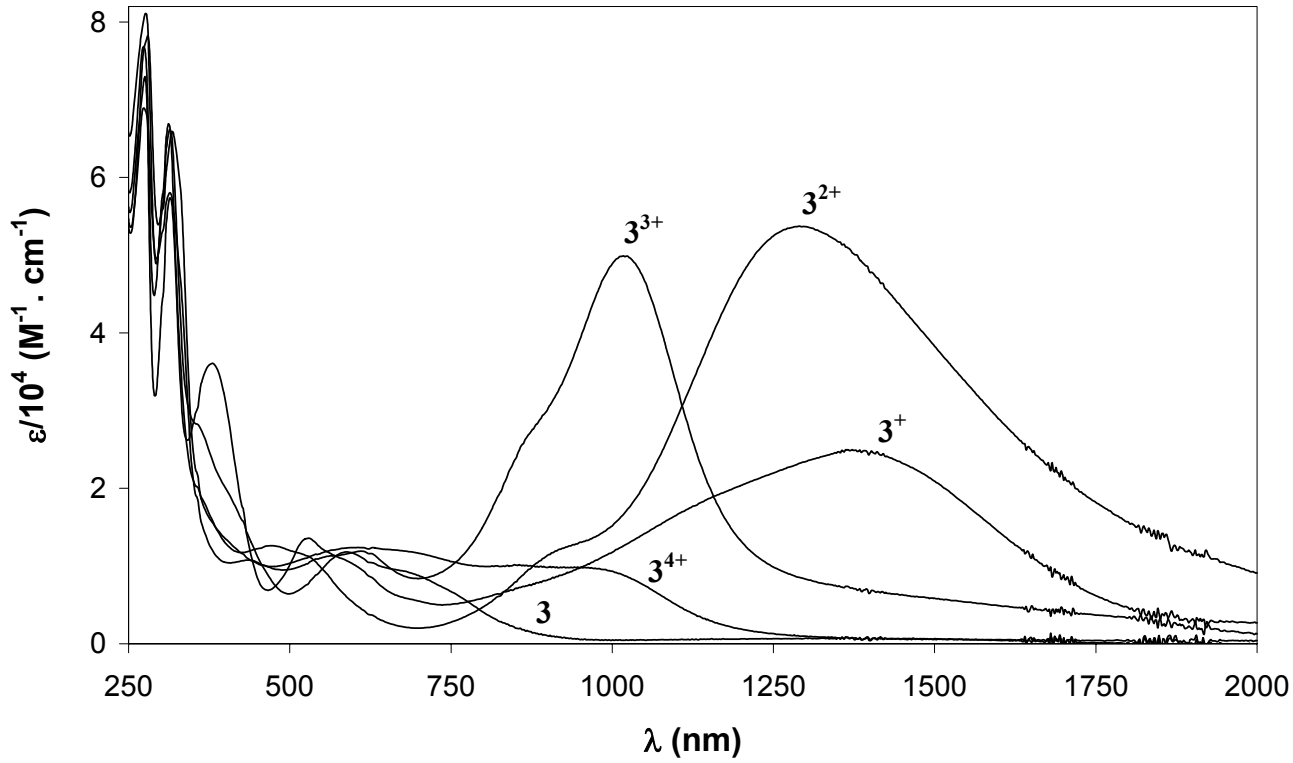

Figure 2. spectroelectrochemical oxydation of **3** in DCM, 0.1M TBAH. (See also Figures S3-S6)

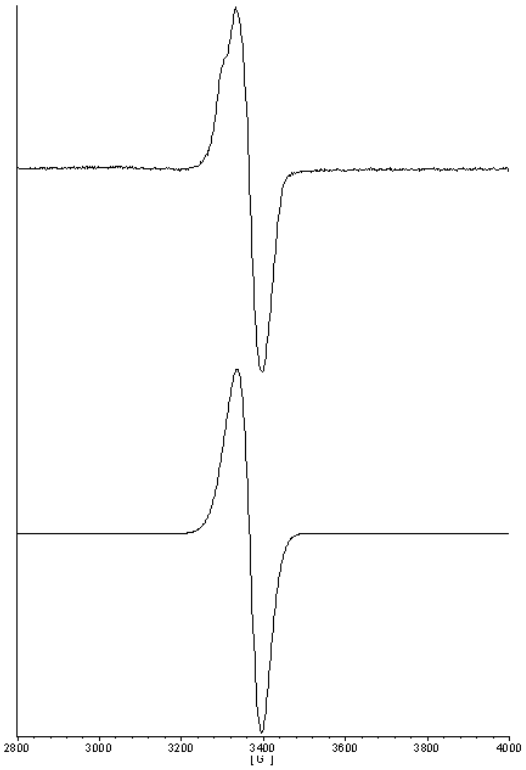

Figure 3. Experimental (top) EPR spectrum of $\mathbf{3}^{+}$ in frozen CH_2Cl_2 (100 K) and simulated (bottom).

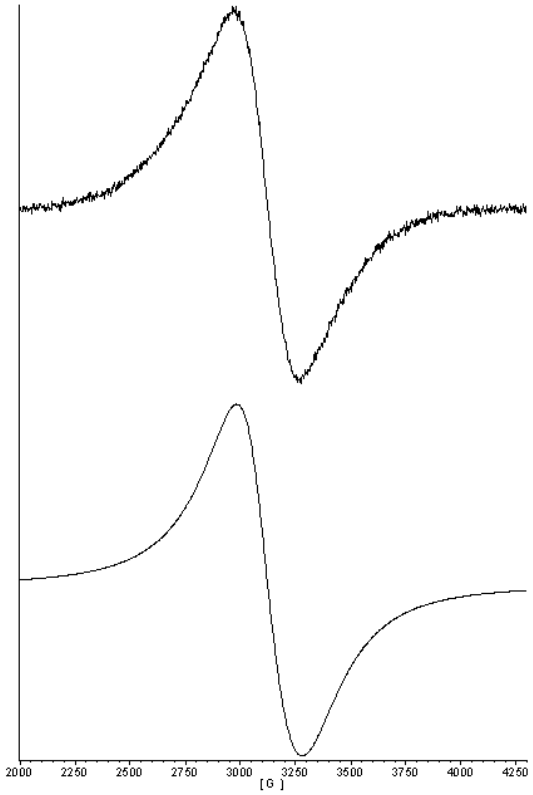

Figure 4. Experimental (top) EPR spectrum of $\mathbf{3}^{3+}$ in frozen CH_2Cl_2 (100 K) and simulated (bottom).

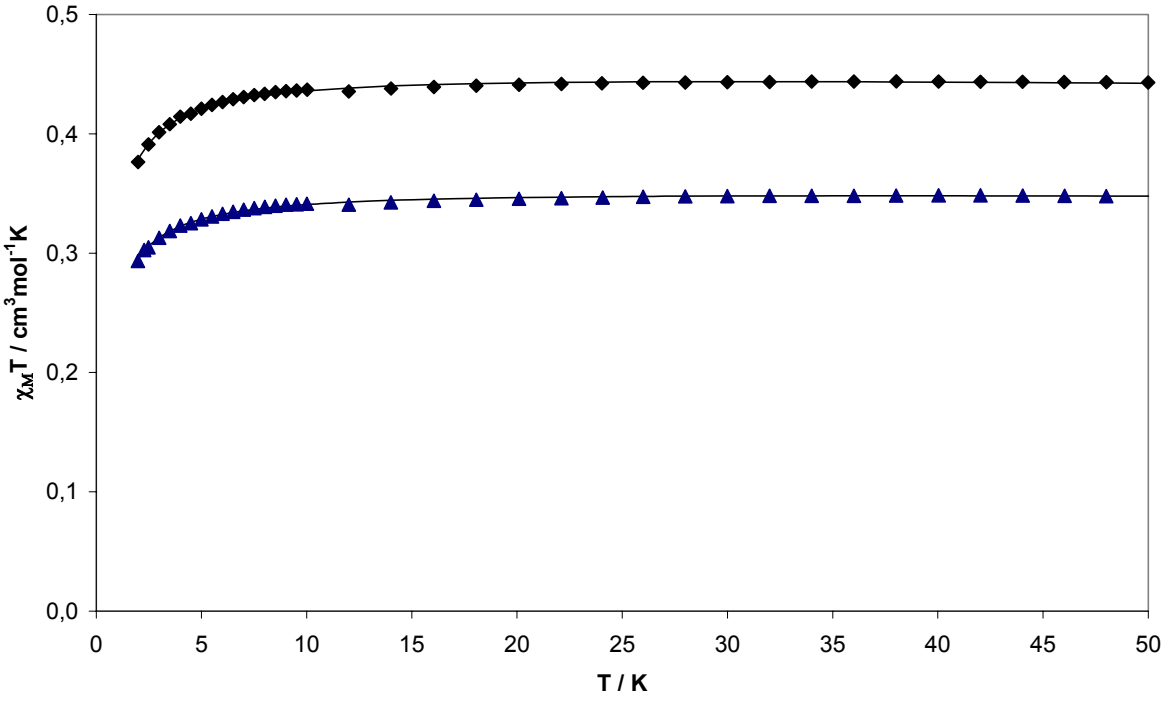

Figure 5. χT versus T recorded on powder samples of [**2**][PF_6] (filled squares) and [**3**][PF_6] (filled triangles) and theoretical laws according to equation 1.

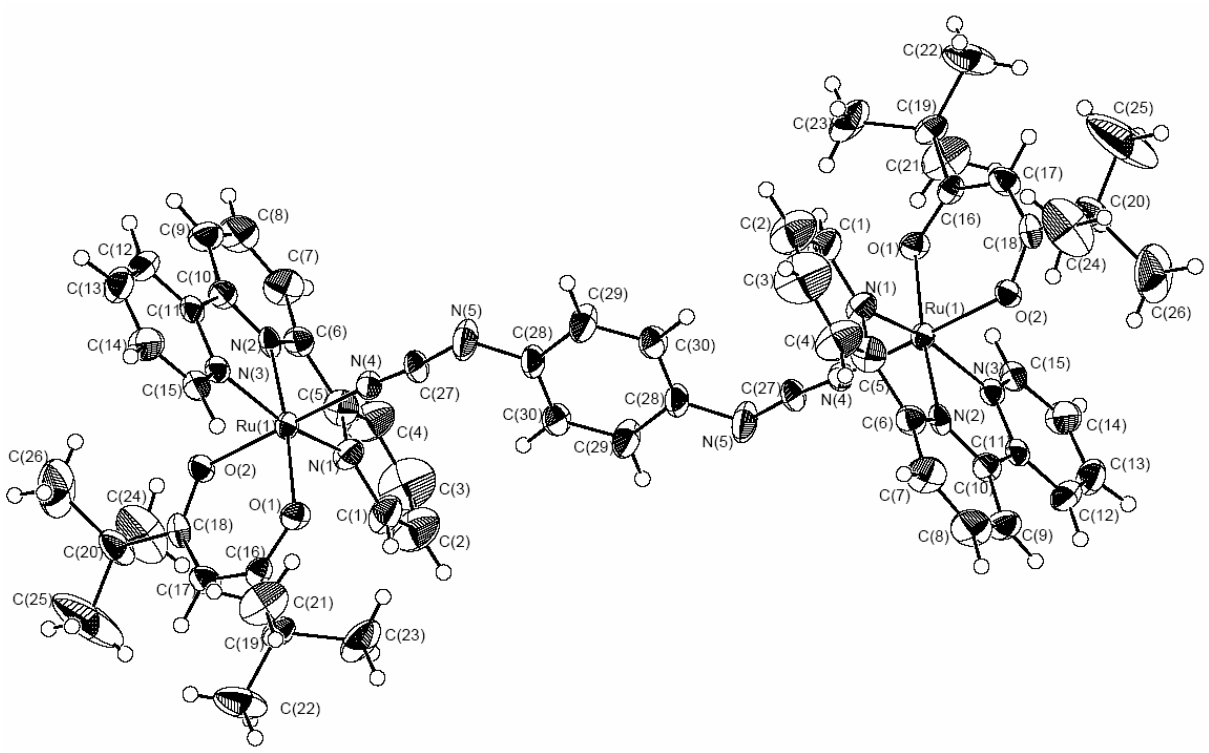

Figure 6. ORTEP drawing of complex [**3**][PF6]$_2$ (conformer A) along with the atom numbering scheme, probability level of 30%.

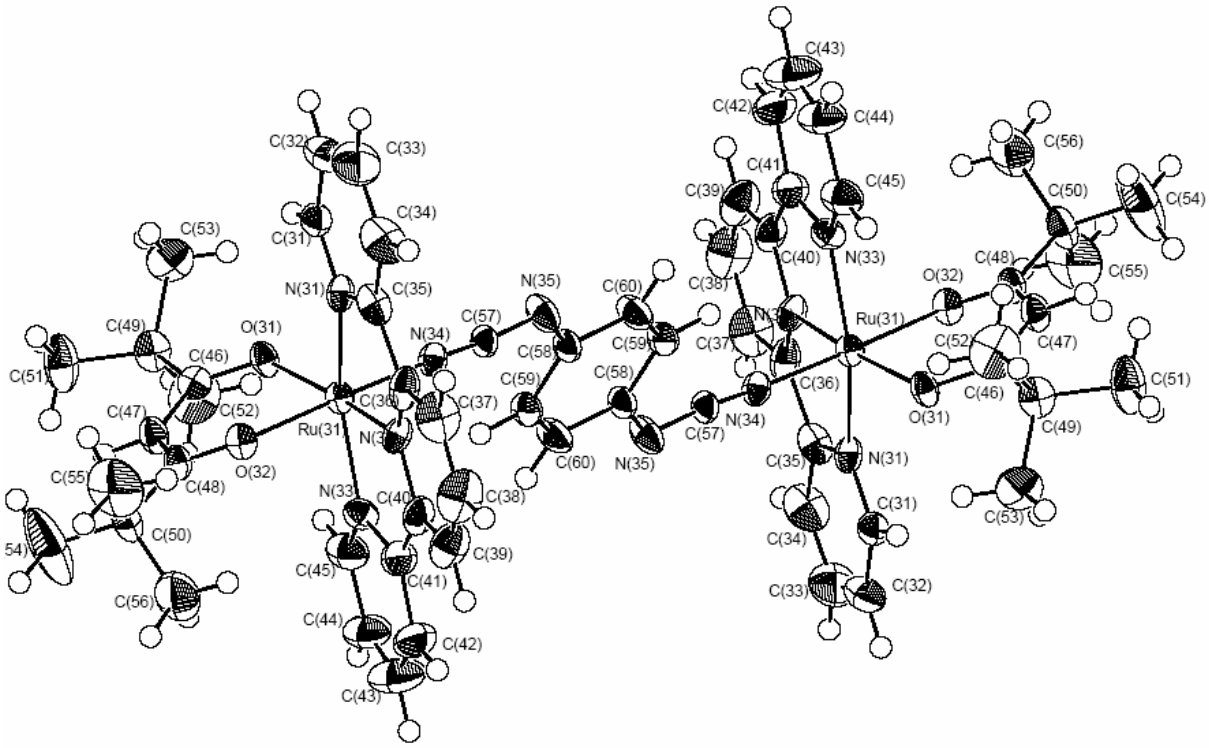

Figure 7. ORTEP drawing of complex [**3**][PF_6]$_2$ (conformer B) along with the atom numbering scheme, probability level of 30%.

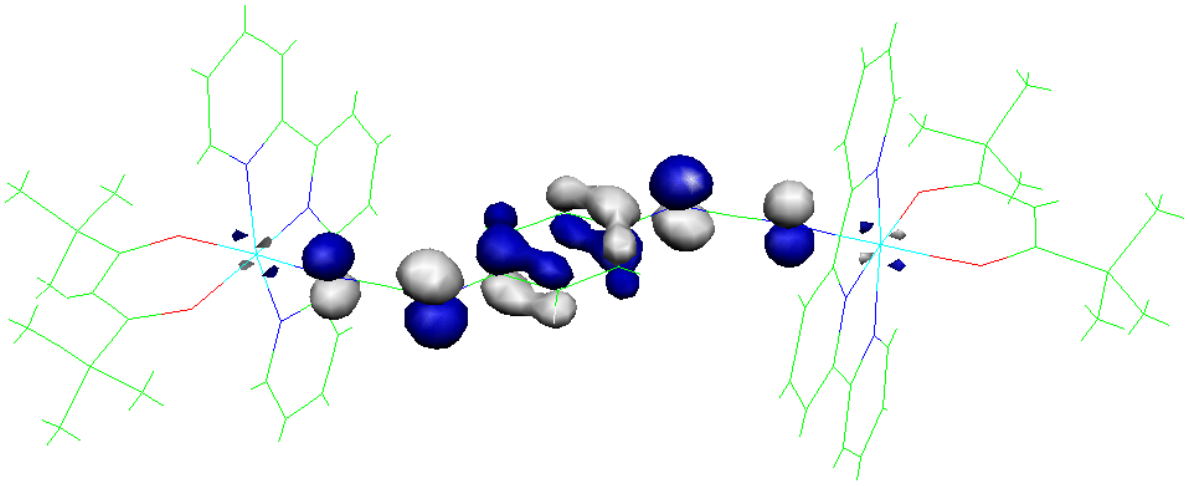

Figure 8. Highest occupied molecular orbital (HOMO) for complex **3.**

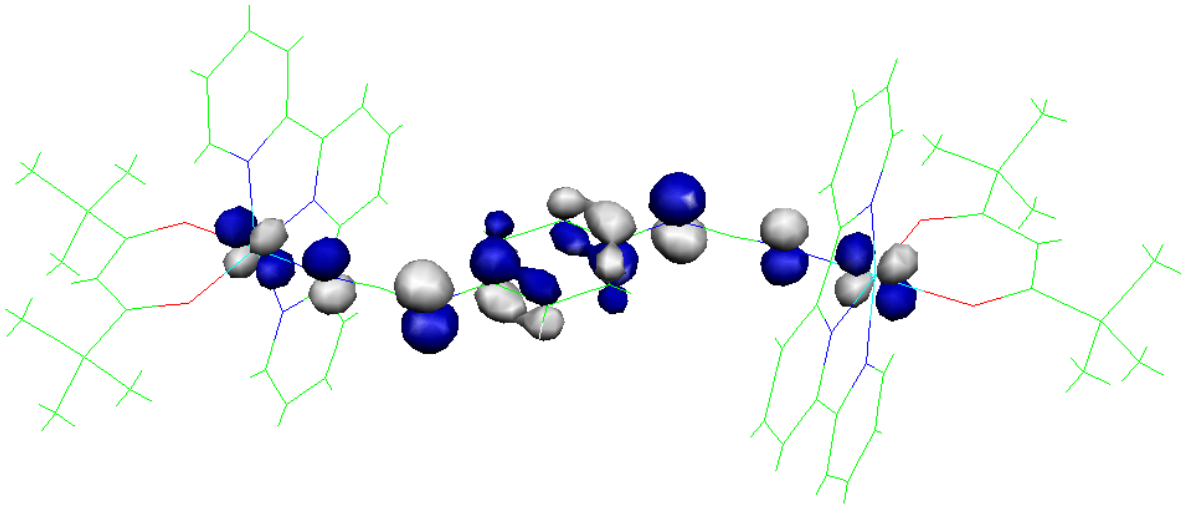

Figure 9. Singly occupied molecular orbital (SOMO) for complex $\mathbf{3}^{+}$.

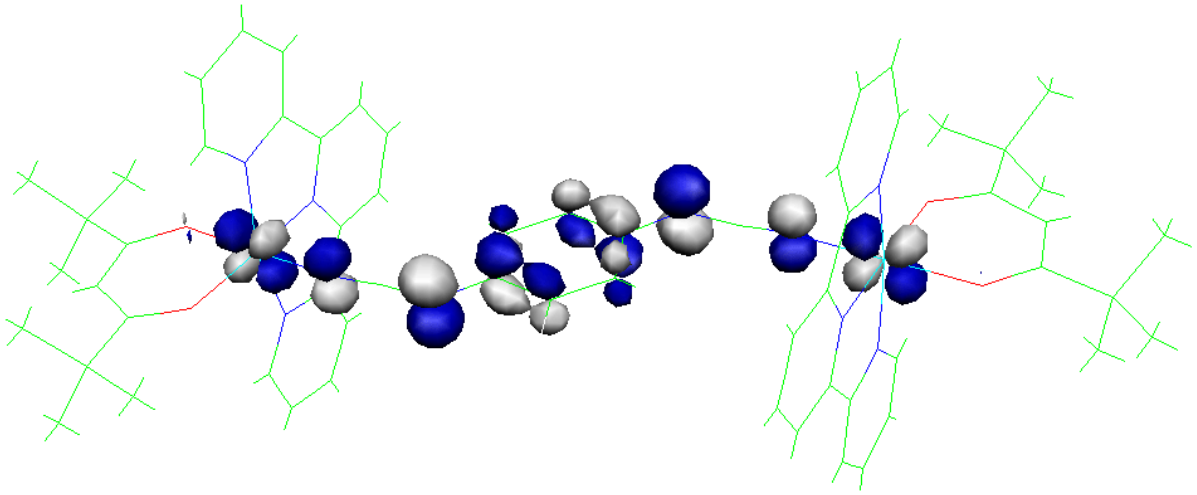

Figure 10. Lowest unoccupied molecular orbital (LUMO) for complex $\mathbf{3}^{2+}$.

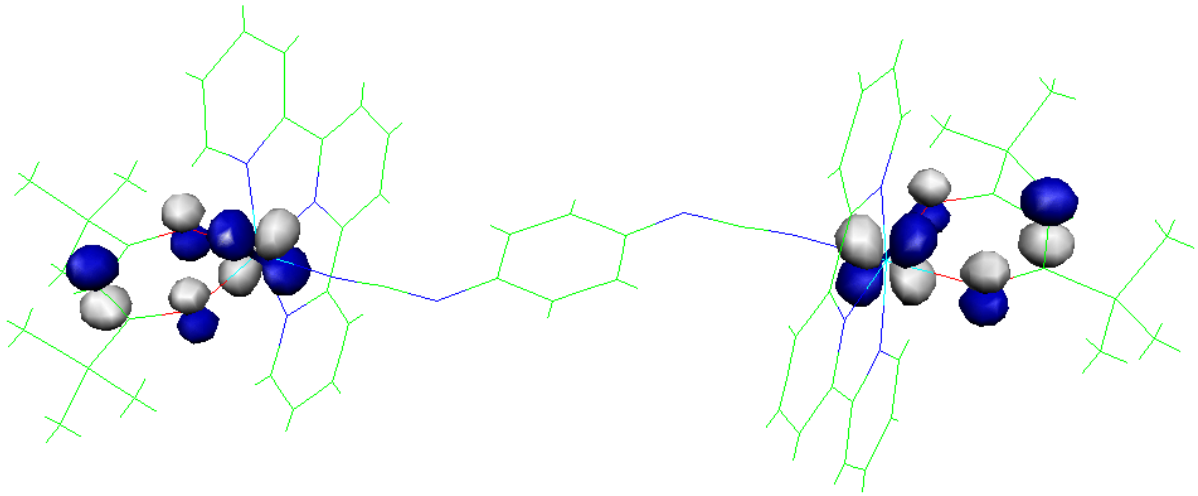

Figure 11. Highest occupied molecular orbital (HOMO) for complex $\mathbf{3}^{2+}$.

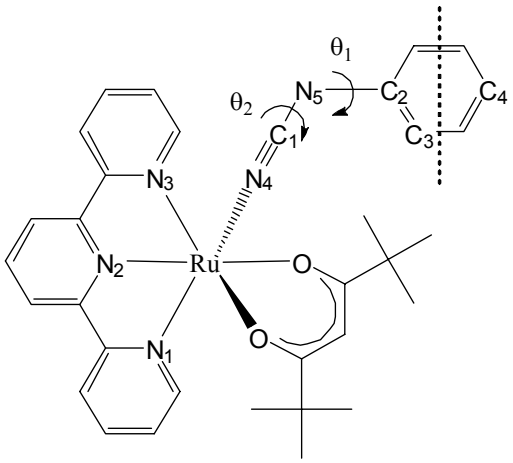

Figure 12. Degrees of freedom of the dinuclear complex. Two possible rotation angles, θ_1 and θ_2 can be identified on each moiety.

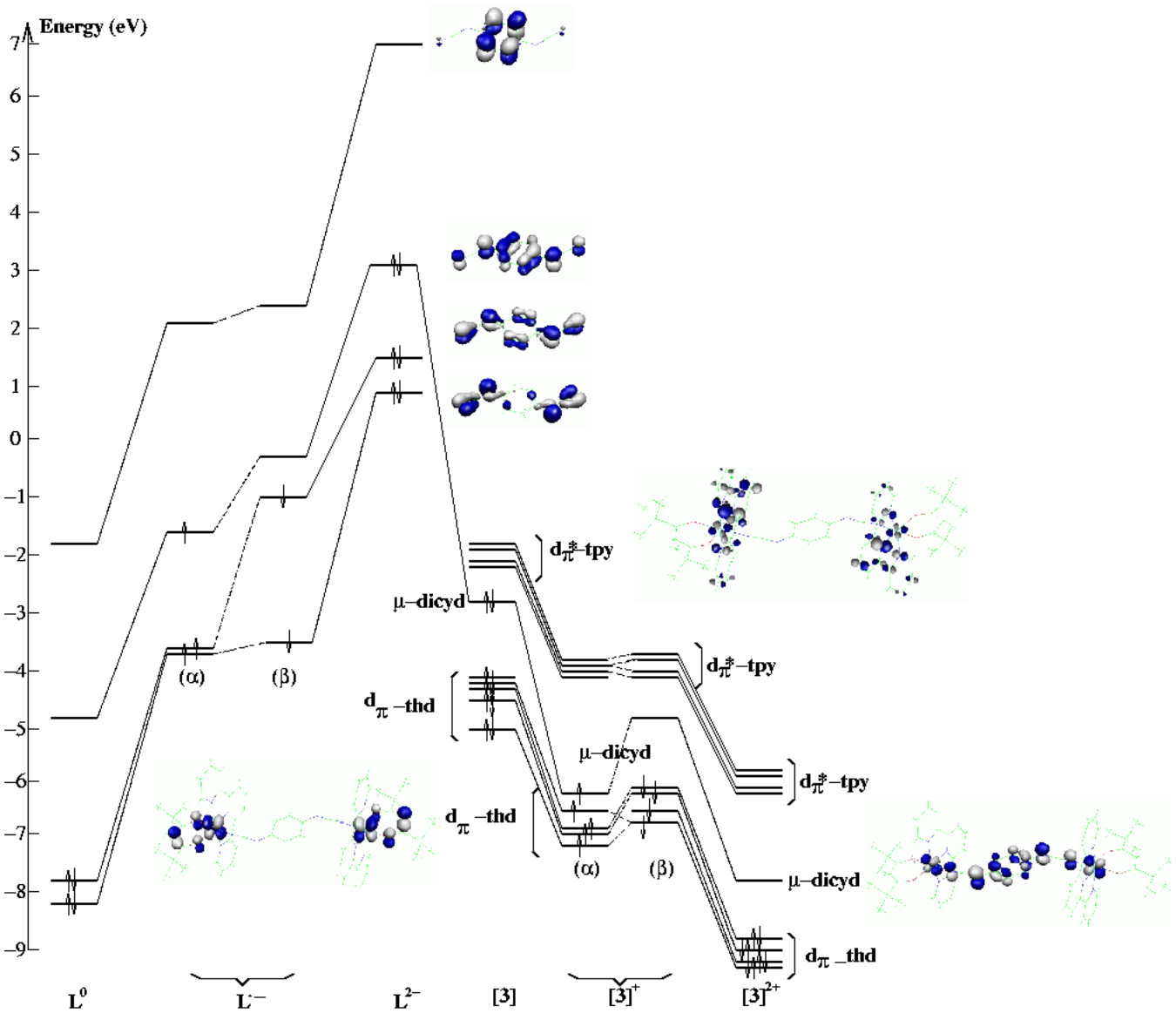

Figure 13. Frontier molecular orbitals correlation diagram for the bridging ligand **L** and the binuclear complex **3** in their first three oxidized states.

For Table of Contents

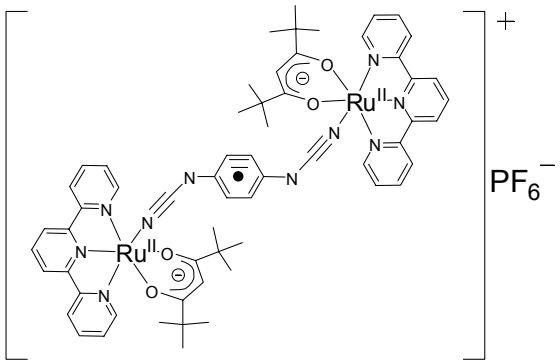

The dicyanamidobenzene-bridge diruthenium complex [{Ru(tpy)(thd)}$_2$(μ-dicyd)] in its monocationic form is found to be a ligand-centered anion radical, and in its dicationic form appears to be an unconventional mixed-valent Ru(II)/Ru(III) system where the electronic interaction occurs through an open shell anion radical ligand as shown by UV/Vis/NIR, EPR spectroscopy, X-Ray, Magnetic susceptibility measurements, and DFT calculations. This clearly shows the non-innocent behavior of the dicyanamidobenzene bridging ligand.